THE OHIO STATE UNIVERSITY

Revolutionizing Turbine Cooling with Micro-Architectures Enabled by Direct Metal Laser Sintering

The Ohio State University
Aerospace Research Center

J.P. Bons, A. Ameri, J. Gregory,
A. Hossain, L. Agricola, E. Asar

(31 Oct 2018 – NETL UTSR Workshop)

ARC

arc.engineering.osu.edu

Research Team

TEAM LEAD
Dr. Jeffrey Bons
Focus: Experimental Fluid Mechanics and Heat Transfer

Co-PI
Dr. Ali Ameri
Focus: Computational Fluid Dynamics and Heat Transfer

Co-PI
Dr. Jim Gregory
Focus: Experimental Fluid Mechanics, Fluidic Oscillator Development

Arif Hossain
Graduate student

Elif Asar
Graduate student

Objectives

- Explore innovative cooling architectures enabled by additive manufacturing techniques for improved cooling performance and reduced coolant waste.
- Leverage DMLS to better distribute coolant through microchannels, as well as to integrate inherently unstable flow devices to enhance internal and external heat transfer.
- Demonstrate these technologies
  1. at large scale and low speed.
  2. at relevant Mach numbers in a high-speed cascade.
  3. finally, at high speed and high temperature.
- Complement experiments with CFD modeling to explore a broader design space and extrapolate to more complex operating conditions.

Turbine Heat Transfer Facilities

- For innovative concepts to be viable, must be vetted in facilities that simulate the real operating environment
- Graduated complexity
  1. Low speed, large scale
  2. High speed, smaller scale
  3. High speed, high temp (T_w/T_b), small scale

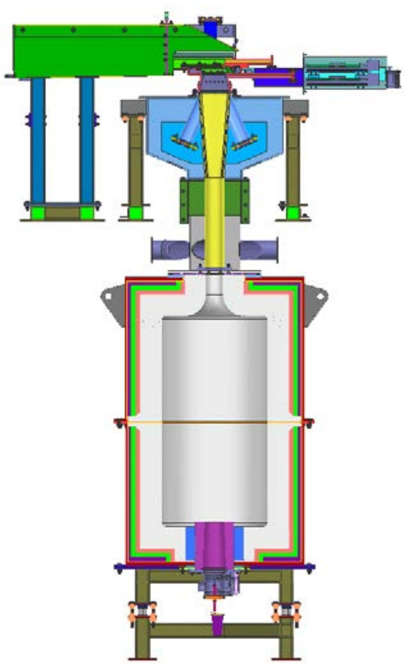

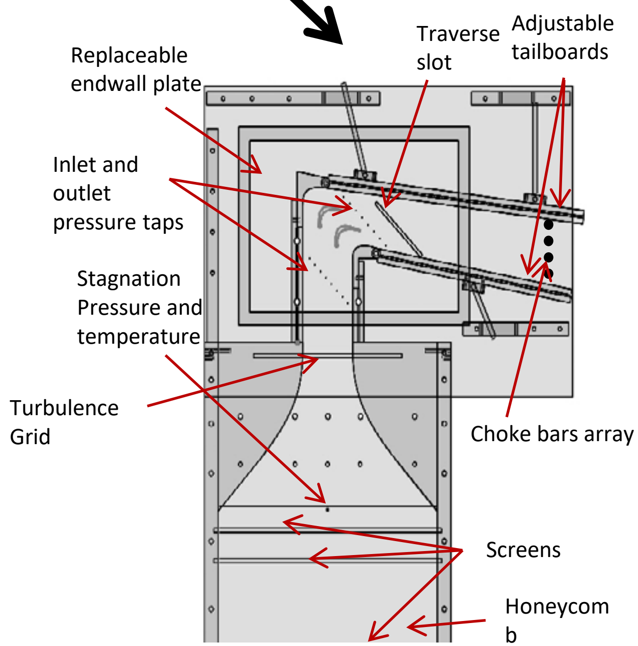

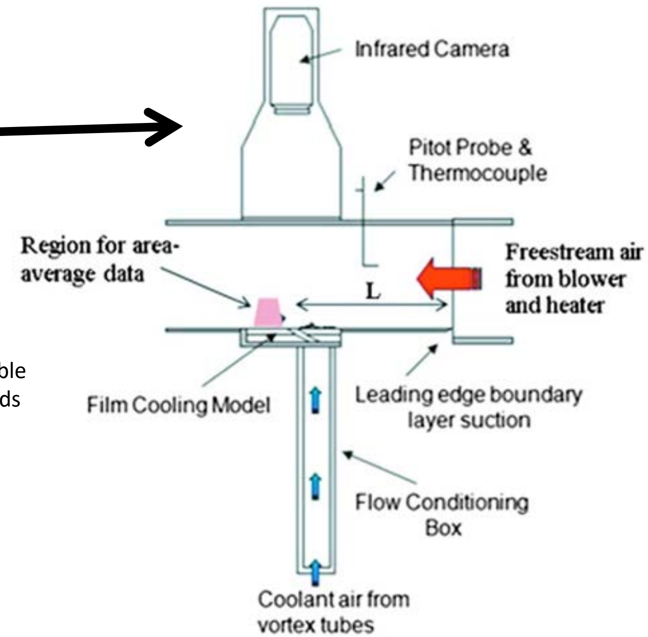

PHASE 2: NGV Design and Development

- **Innovative cooling architectures** tested:
  - Sweeping jet for external film cooling for suction surface TODAY
  - Truncated pin fin array for trailing edge cooling TODAY
  - Sweeping jet impingement for internal cooling of leading edges TODAY
  - Reverse flow film cooling for pressure surface LAST YEAR
- **Facility Development and Testing** since last year:
  - Low speed cascade vane with TE cooling
  - New transonic vane cascade
  - Testing with sweeping jets and TE cooling in transonic cascade
- **Develop and use computational models** of each cooling design
  - Validate solutions with experimental data from initial geometry
  - Explore design space and aid in optimization of geometry for each design

Sweeping Jet Film Cooling

Test Conditions

- **Low speed cascade at high blowing ratio ($1<M<3.25$)**
- **Transonic cascade**

Fluidic Oscillator

- ❑ Pressurized fluid is introduced into the **power nozzle** along the centerline of the throat.
- ❑ As the intensity of the vortices increases the power stream deflects to the side wall due to the **Coanda effect**.
- ❑ This allows a portion of the fluid to enter into the **feedback loop** which flows back to the control port and causes the power stream to **detach from the side wall**.
- ❑ The power stream then **switches to the opposite wall** and the same process repeats, resulting in an oscillatory fluid motion at the throat.

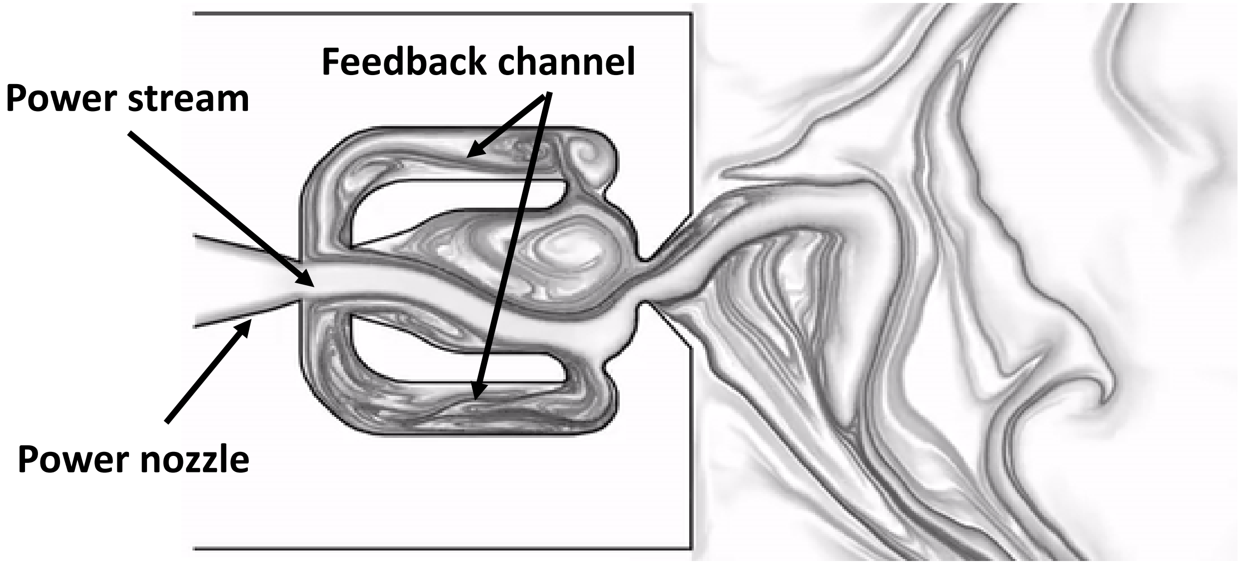

(Ostermann et al. 2015)

Current Application

- ❑ Drag reduction
- ❑ Flow control
- ❑ Windshield spray
- ❑ Noise reduction

OSU Application

- ❑ Film cooling
- ❑ Impingement cooling

Low Speed Cascade Design

- Tests performed in a linear cascade in an open-loop wind tunnel
- The linear cascade section consists of three-vanes, two passages.
- Tunnel can be operated up to 14.3% turbulence intensity.

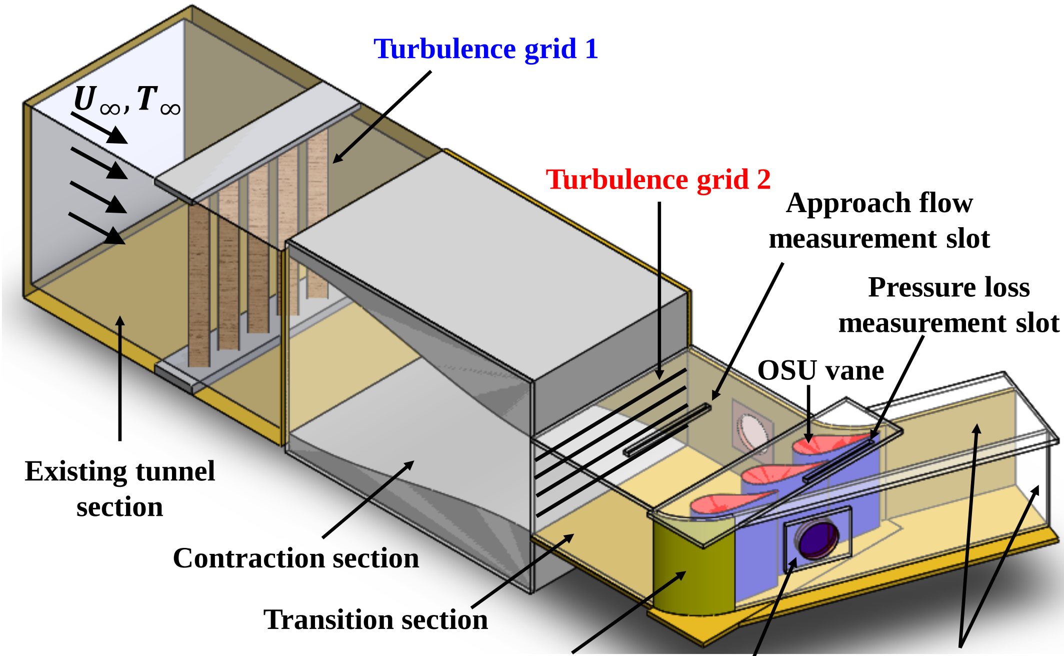

Vane geometry and flow condition

Parameter	Value
True chord (C)	$15.24cm(6in)$
Axial chord (C_x)	$8.33cm(3.28in)$
Chord/pitch (C/P)	1.20
Span/chord (S/C)	1.25
Inlet and exit angles	$0°$ and $70°$
Chord Reynolds number (Re_{in})	9.5×10^4
Freestream velocity, (U_∞)	$9.5m/s$
Freestream temperature, (T_∞)	$315K$

Turbulence condition

Turbulence grid	Turbulence intensity (Tu)	Length scale (Λ_f)	Thermal uniformity
No grid	0.6%	-	±1.5K
Grid 1	6.3%	15.6mm (6D)	±0.75K
Grid 2	14.3%	42.5 mm (17D)	±1.0K
Grid 1+Grid 2	14.3%	35mm (14D)	±0.5K

Vane Geometry

- The turbine vane (**OSU vane**) used in this study was designed and manufactured at the Turbine Aerothermodynamics Lab.
- high resolution **Stereolithography (SLA)** technique was used to manufacture the vane modules with **Accura ABS Black**.

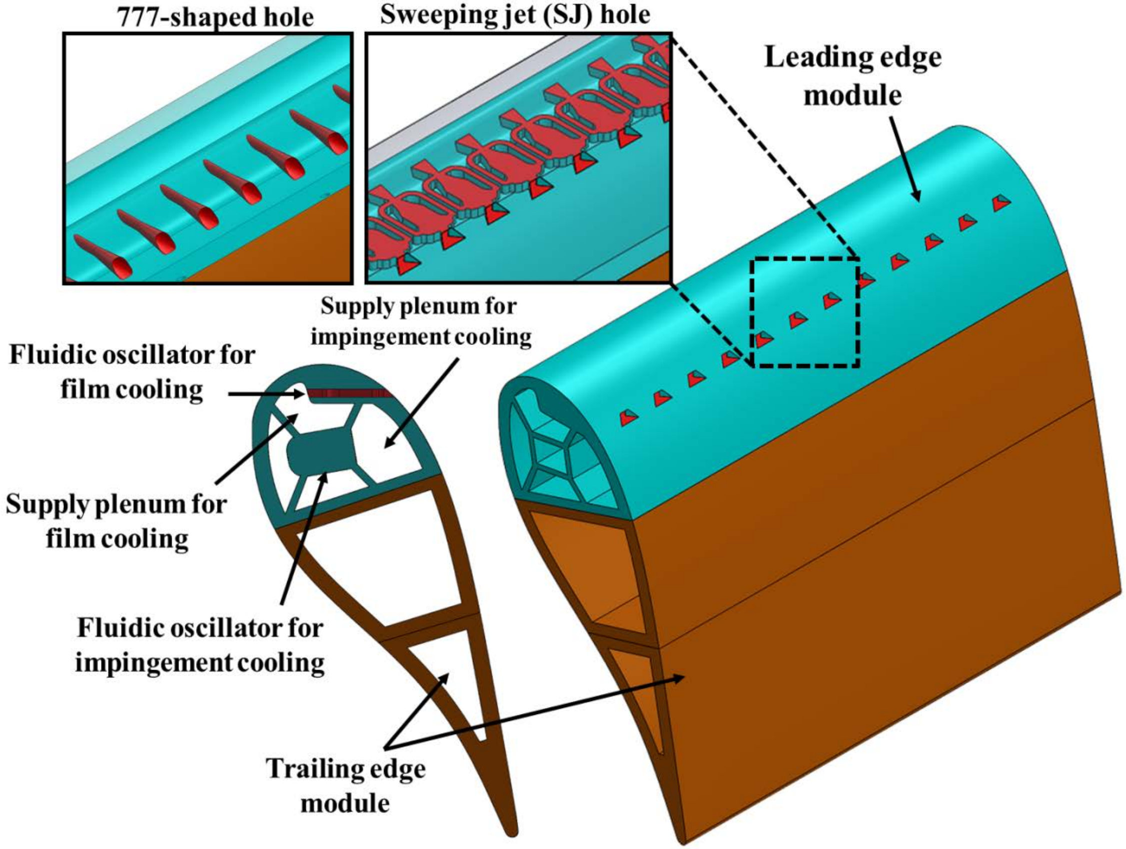

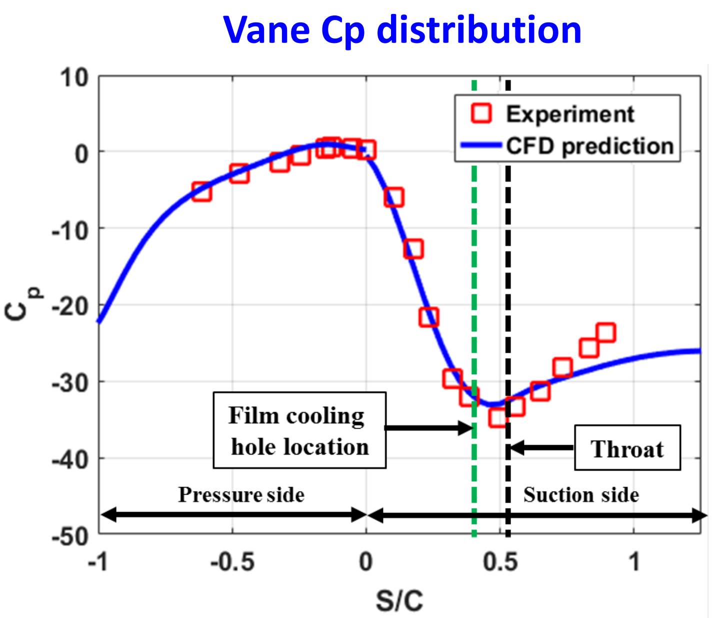

Adiabatic Film Effectiveness (Tu = 0.6%)

- **Strong periodicity** was observed for both SJ and 777-hole.
- Due to the **sweeping action** of the jet, a **higher effectiveness** value was observed in the lateral direction for SJ hole compared to 777- hole at **M = 3**.

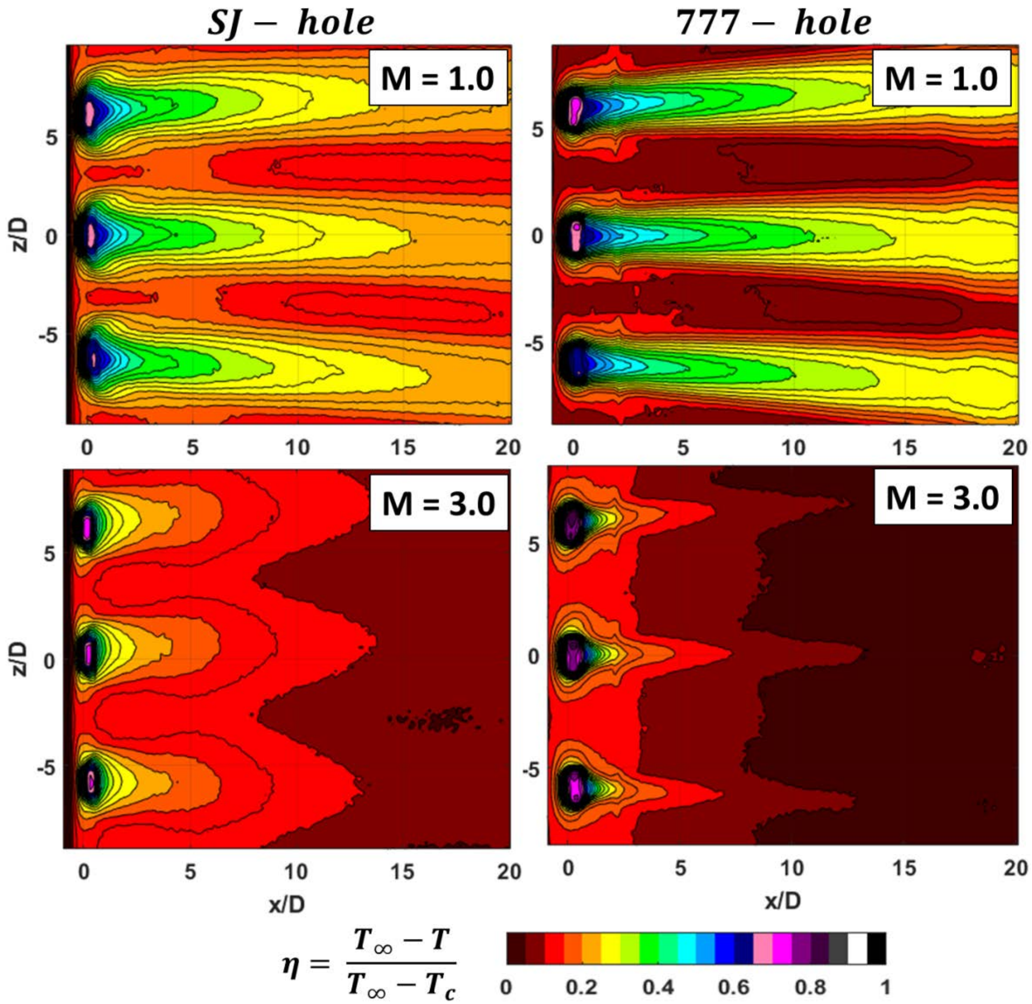

$$\eta = \frac{T_\infty - T}{T_\infty - T_c}$$

Adiabatic Film Effectiveness (Tu = 14.3%)

- The freestream turbulence **increases mixing** thus the film **effectiveness drops.**
- However, the **lateral spreading** of the coolant **increases with freestream turbulence** for **777-hole** which is not uncommon for steady film cooling holes.

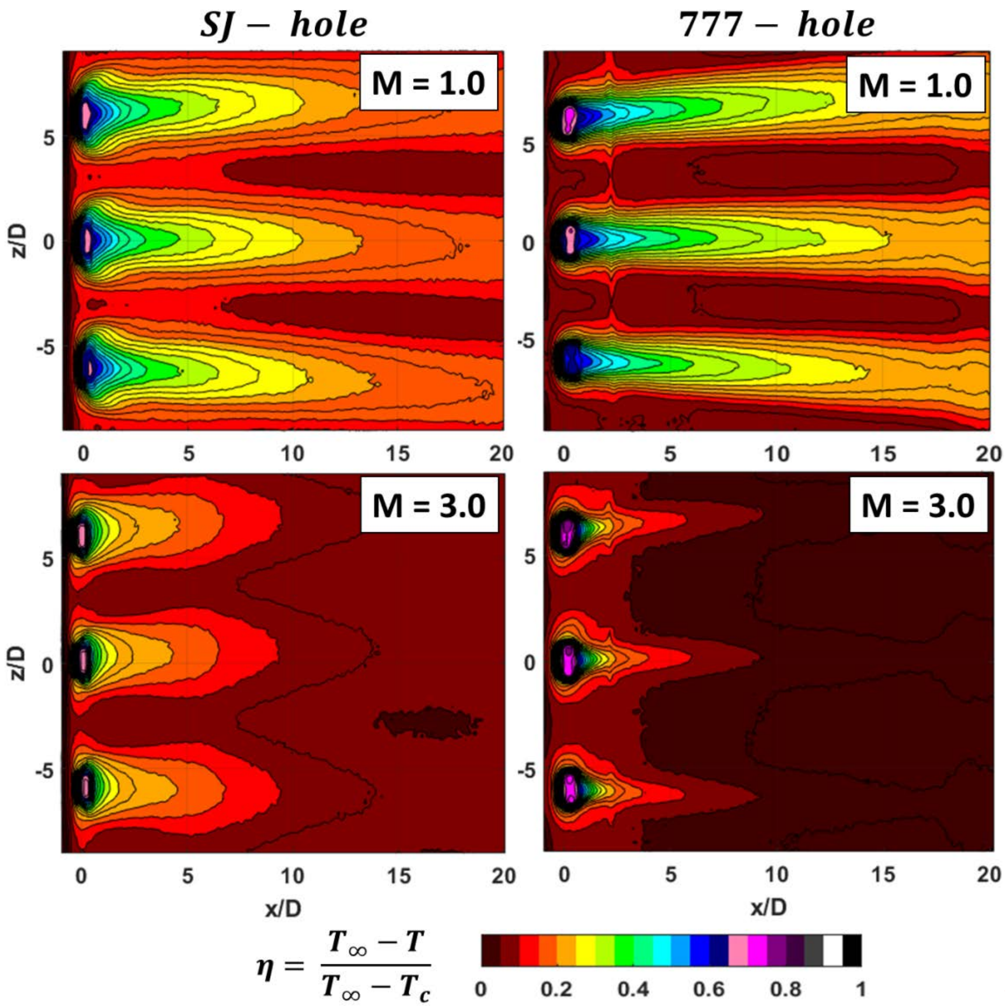

$$\eta = \frac{T_\infty - T}{T_\infty - T_c}$$

Area Averaged Effectiveness

- Data are averaged over **three pitches (18D)** in the spanwise direction and 20D in the streamwise direction.
- The **maximum cooling effectiveness** for both holes can be found **at blowing ratio M = 1**.
- Sweeping jet hole exhibits a **high ($\bar{\bar{\eta}}$)** at high blowing ratio (**M>1**).

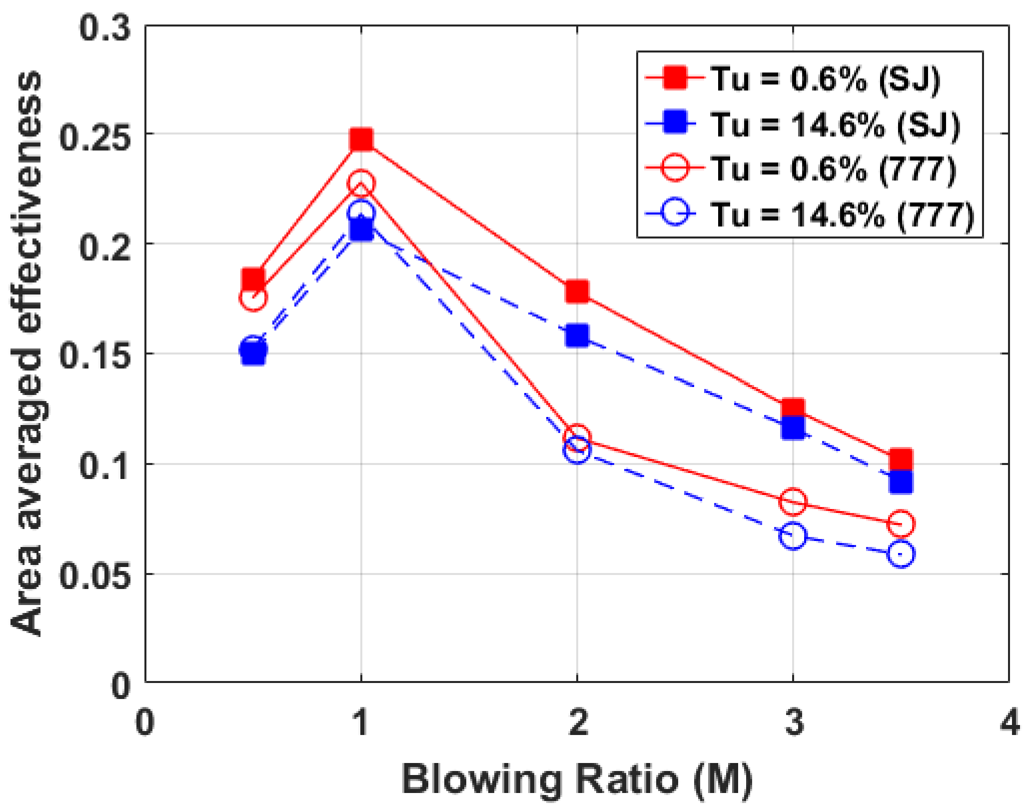

Time Averaged Thermal Field

- Thermal field was measured at a crossplane at x/D = 12.
- The thermal field revealed that the lateral spreading of coolant is much wider for the SJ hole while the coolant spreading drops significantly for the 777-hole at **M = 3**

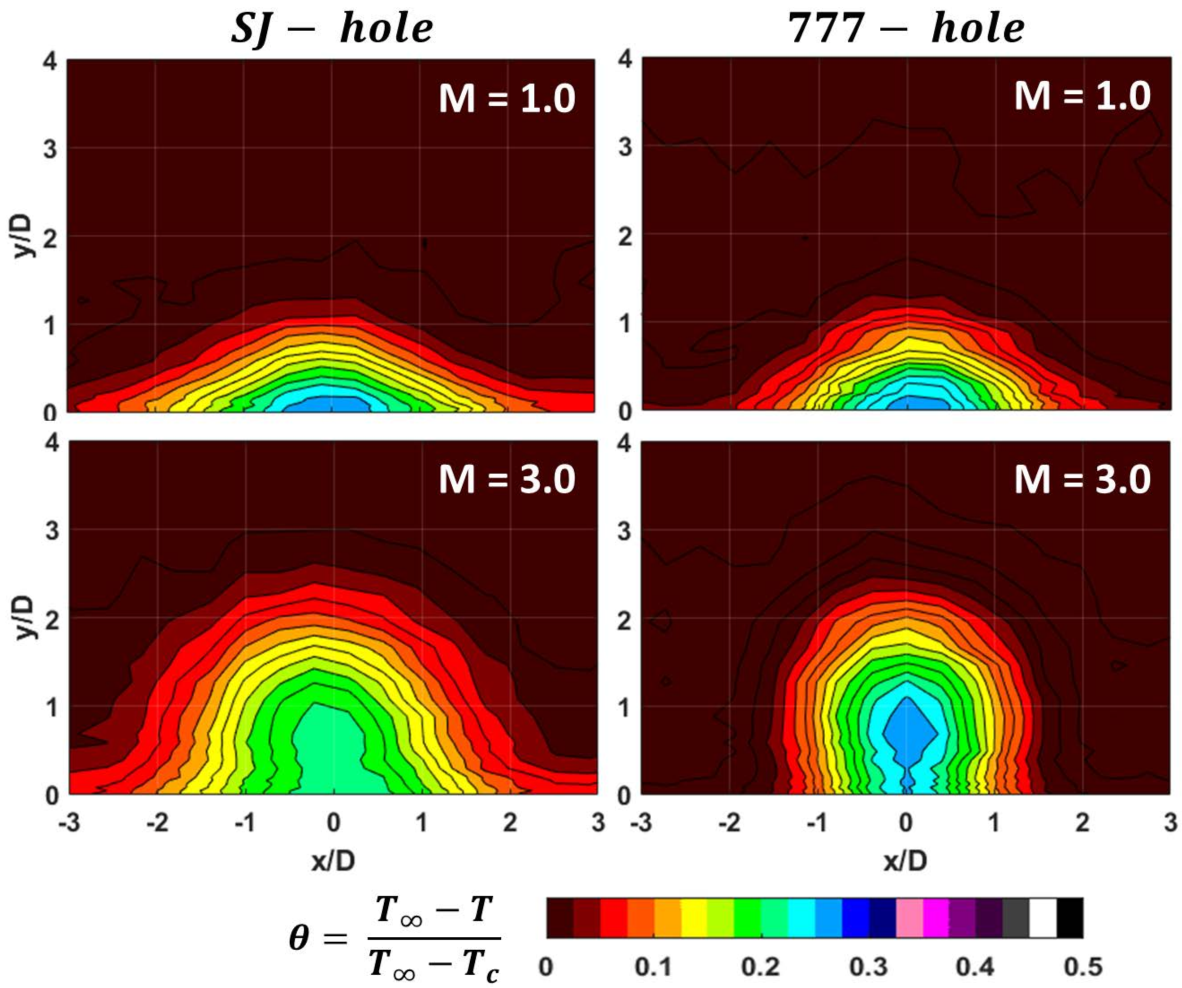

$$\theta = \frac{T_\infty - T}{T_\infty - T_c}$$

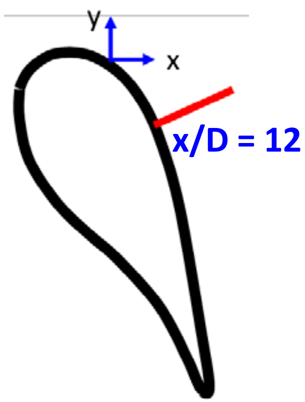

Computational Study (Large Eddy Simulation)

- LES calculations were performed using commercial finite volume solver FLUENT.
- A wall adapting local eddy viscosity (**WALE**) model was used as a subgrid scale (SGS) model.

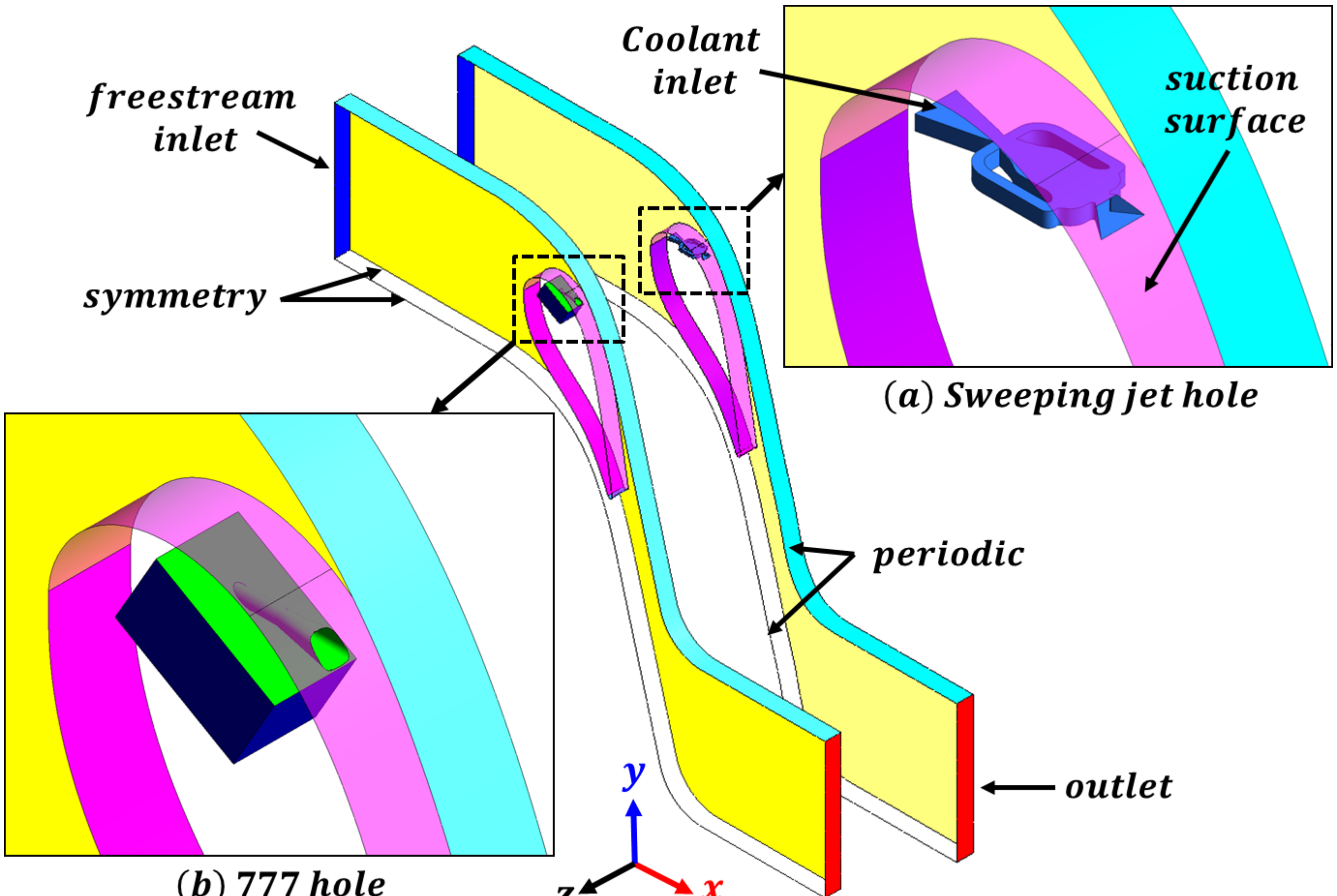

(a) Sweeping jet hole

(b) 777 hole

Time Averaged Velocity Field

- The 777-hole shows a strong jetting action at the hole exit that penetrates high into the freestream.
- This jetting action occurs due to a recirculation zone located at the bottom of the diffuser.
- The SJ hole does not show this type of recirculation at the metering section. Thus, the coolant jet has a lower effective jet momentum.

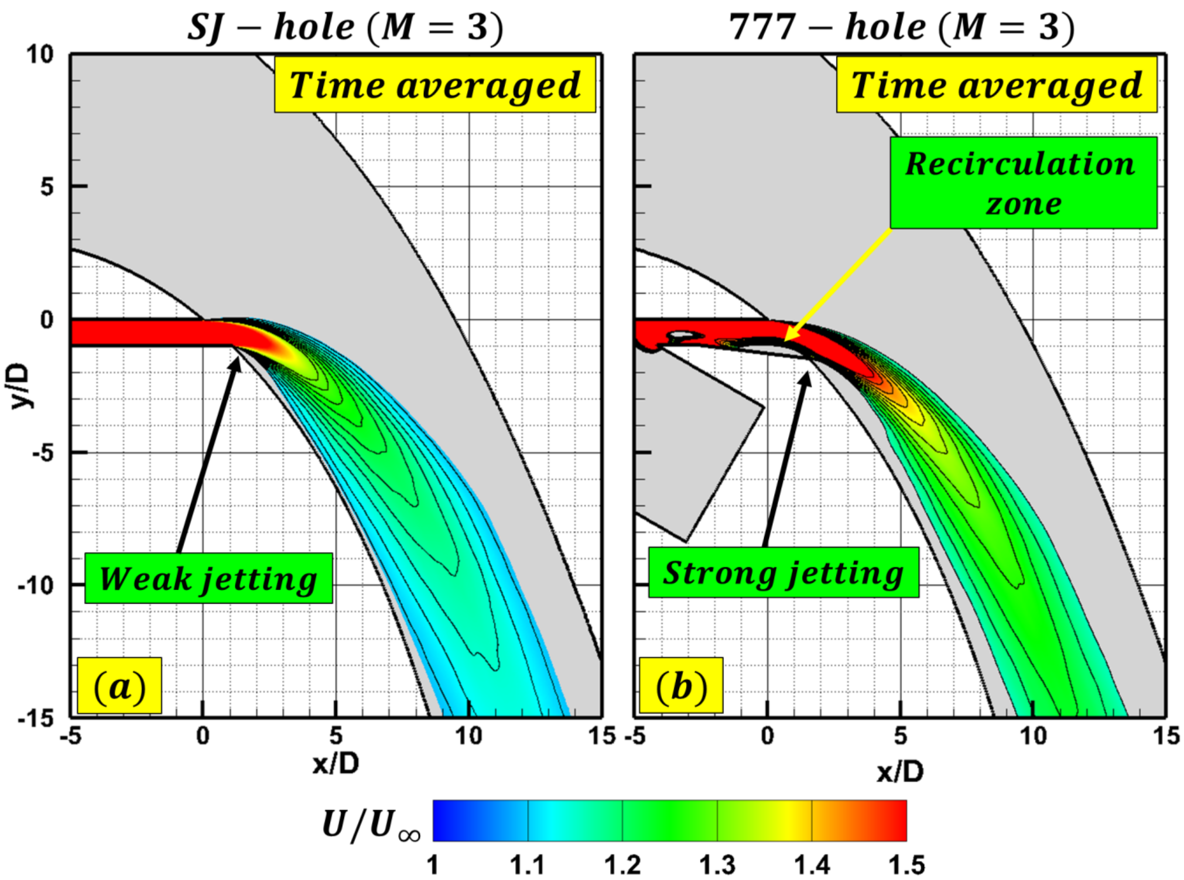

Crossplane Flowfield (x/D = 4)

- The SJ hole shows slightly higher turbulence far downstream of the hole.
- This increased level of turbulence is attributed to the sweeping motion of the jet.
- As the sweeping jet convects downstream, the transverse (spanwise) component (w') of the velocity dominants and becomes a major contributor to the downstream turbulence enhancement.

Crossplane velocity fluctuation (x/D = 4)

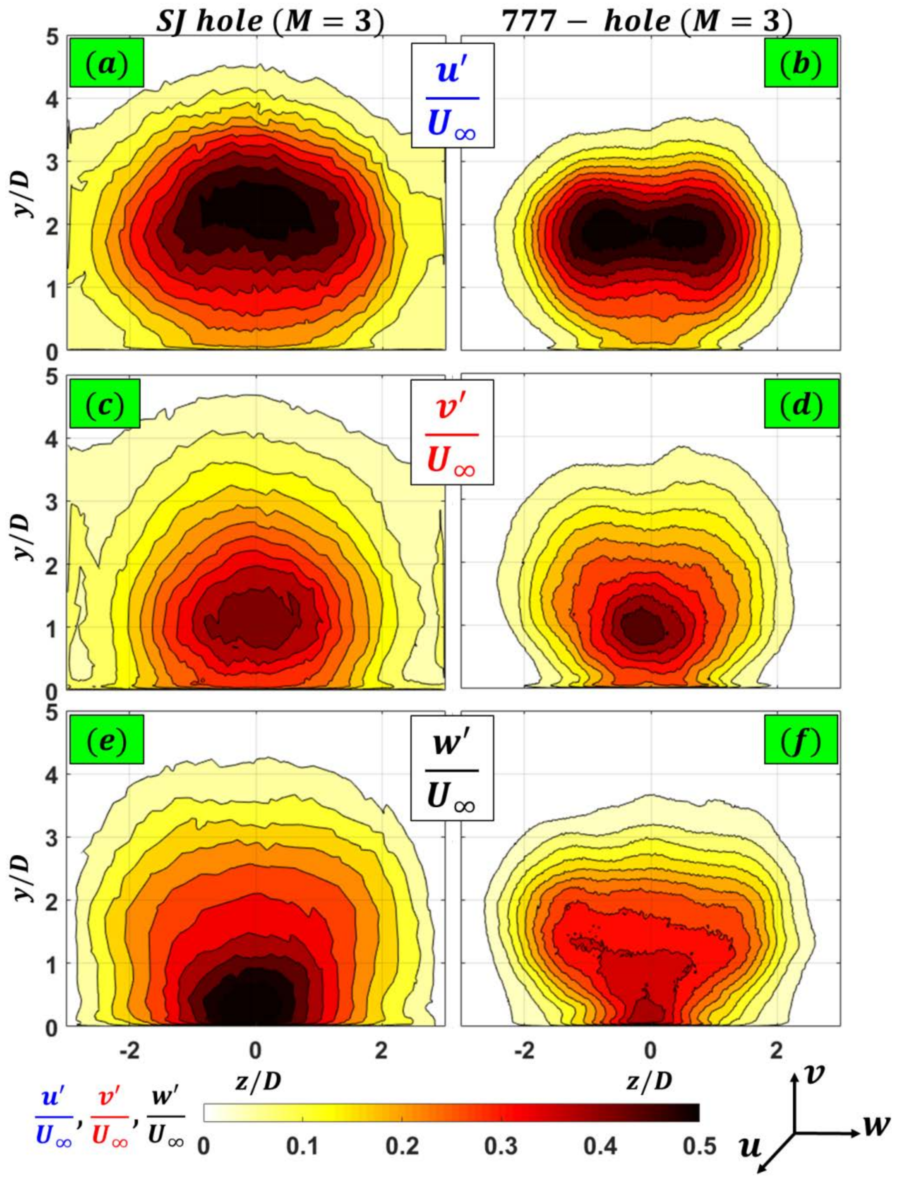

Transonic Cascade Design

- A transonic cascade facility has been developed to achieve the engine Mach number condition.
- The cascade section consists of three-vanes, two passages with optical access.

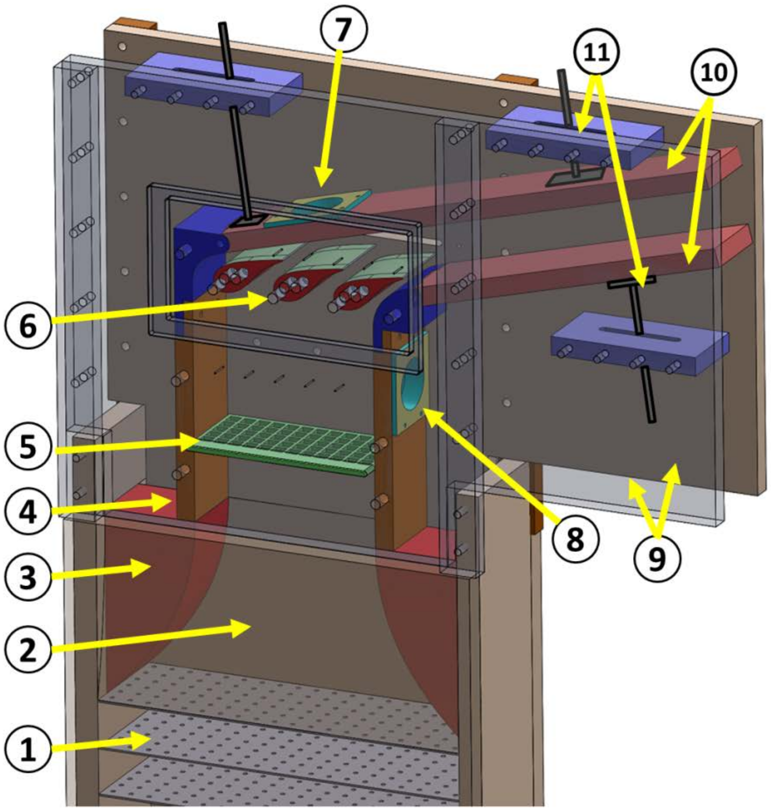

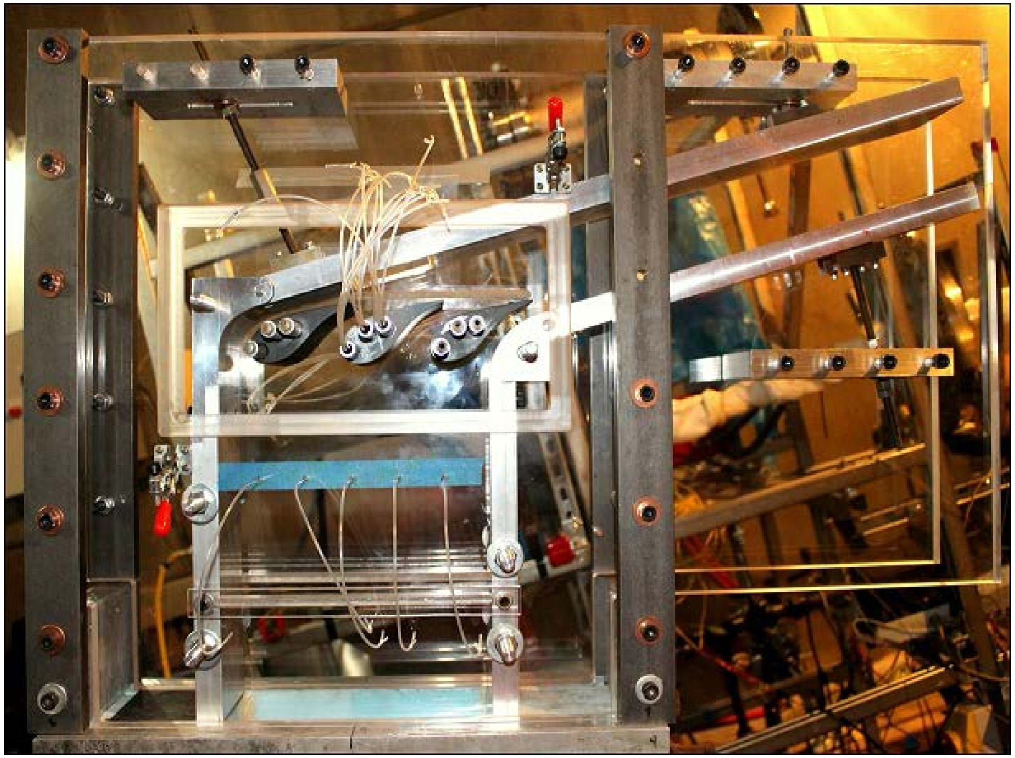

1. Inlet plenum screen
2. Inlet transition
3. Foam contraction
4. Inlet side walls
5. Turbulence grid
6. Vane geometry
7. IR view port for suction surface
8. IR view port for pressure surface
9. End plates
10. Adjustable tailboard
11. Support structure

Transonic Cascade Characterization

- A constant temperature hot film probe was used to measure the turbulence intensity at 1C upstream of the vane leading edge.

Vane geometry and flow condition

Parameter	Value
True Chord (C)	4 *in*
Axial chord (Cx)	2.15 *in*
Chord/Pitch (C/P)	1.20
Span/Chord (S/C)	1.00
Inlet and Exit angle	75°
Exit Reynolds number (Re_{ex})	1.06x106
Exit Mach number (M_{ex})	**0.80**

Turbulence Intensity and Length Scale

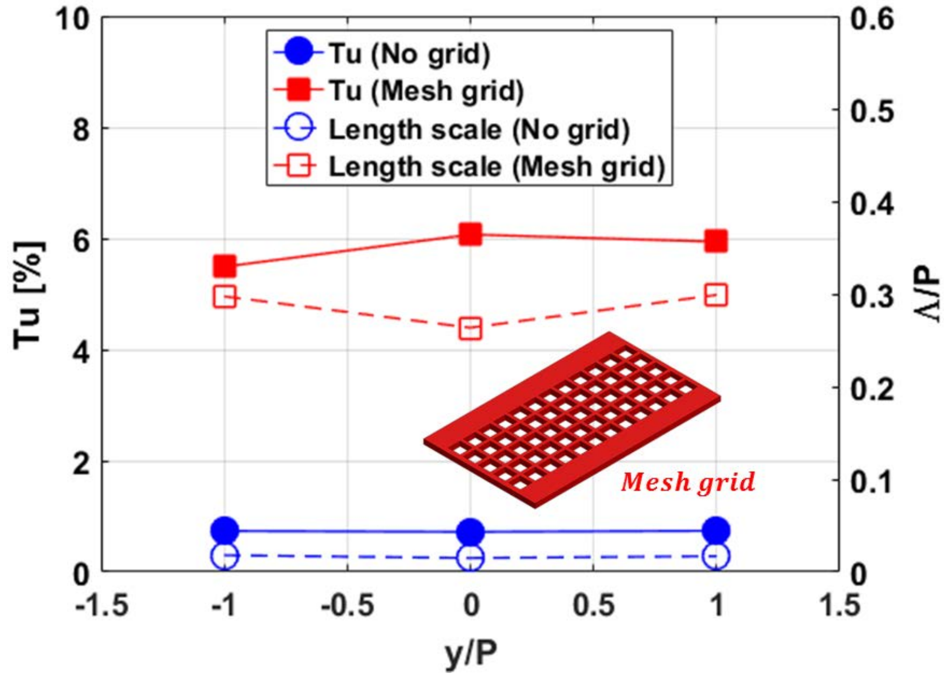

Transonic Vane Geometry

- ❑ Two separate vane geometries (baseline vane and vane with advanced cooling concept) were manufactured.
- ❑ A microphone was used to measured the oscillation frequency of the sweeping jet hole.

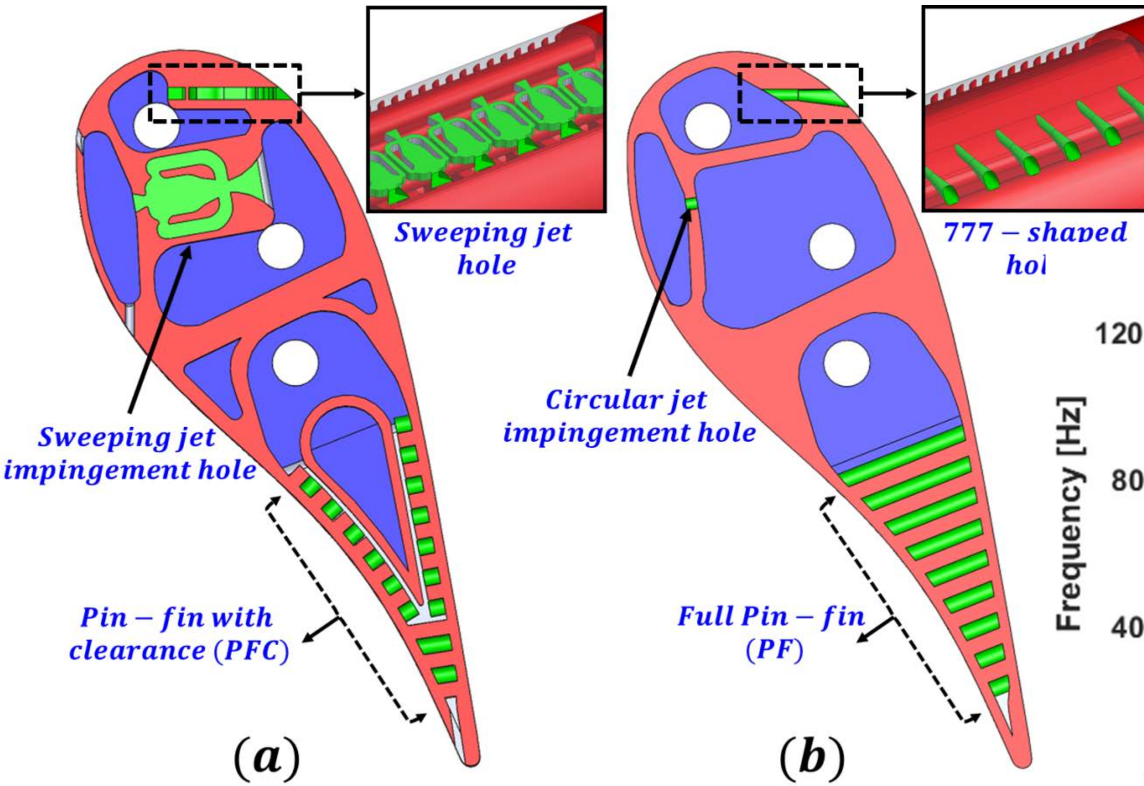

Additively manufactured (SLA) vane geometry

Hole diameter = 1.71mm

Oscillation frequency for SJ vane

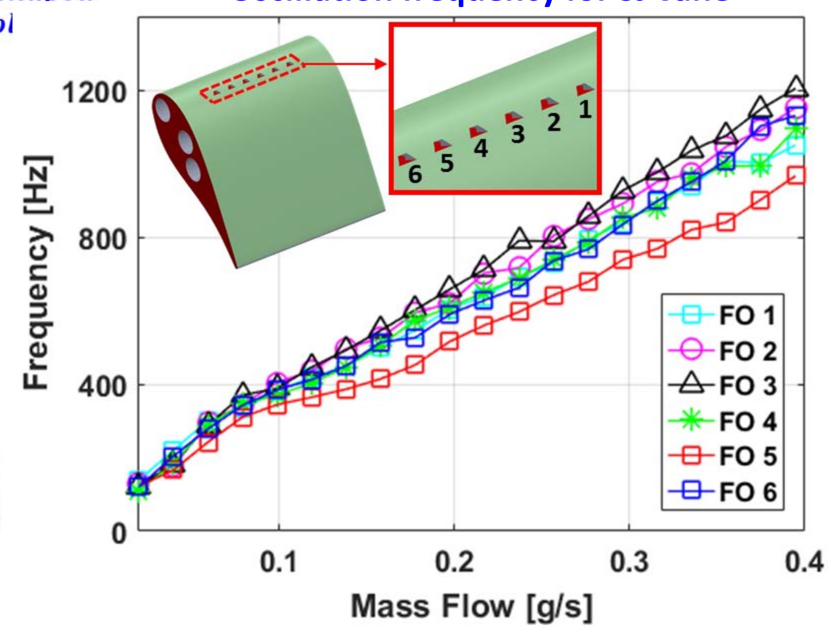

Hole Discharge Coefficient

- The discharge coefficient was measured for the SJ hole and compared with the baseline 777-hole and fan shaped hole.

$$C_d = \frac{\dot{m}_c}{P_{tc}\left(\frac{P_s}{P_{tc}}\right)^{\frac{\gamma+1}{2\gamma}}\sqrt{\frac{2\gamma}{(\gamma-1)RT_{tc}}\left(\left(\frac{P_{tc}}{P_s}\right)^{\frac{\gamma-1}{\gamma}}-1\right)}\frac{\pi}{4}D^2}$$ (Gritsch et al, 1998)

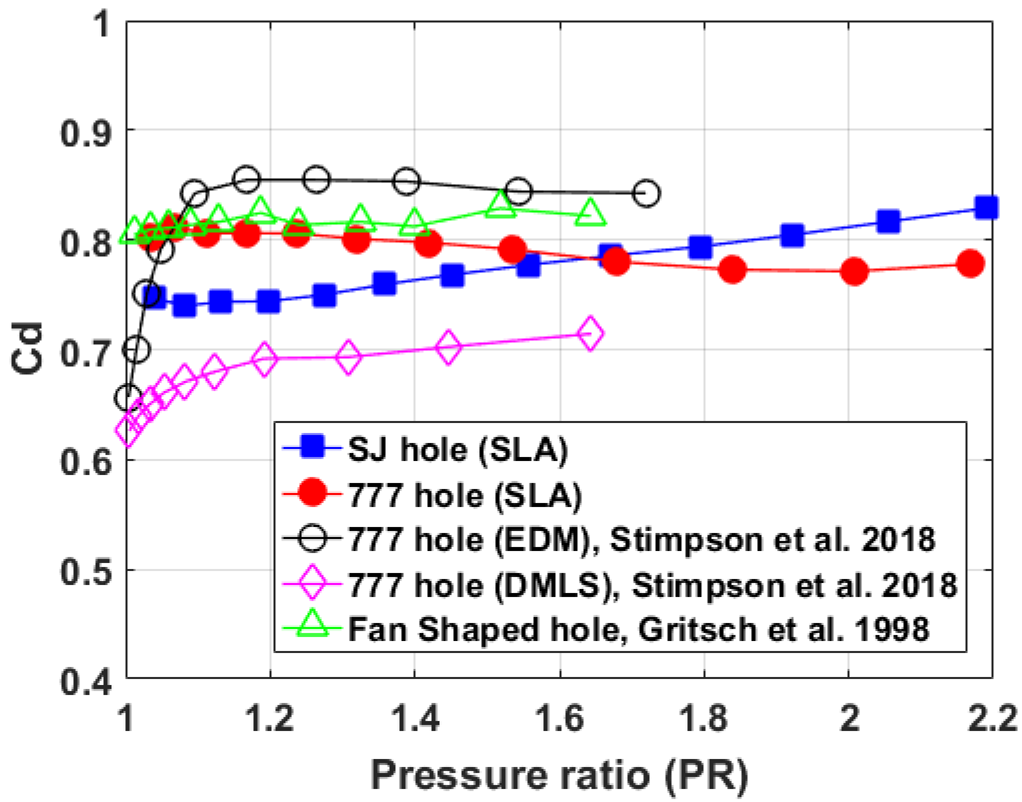

Experimental Measurement

- Experiments were performed at an exit Mach number of 0.8 for a range of blowing ratios.

Measurement locations

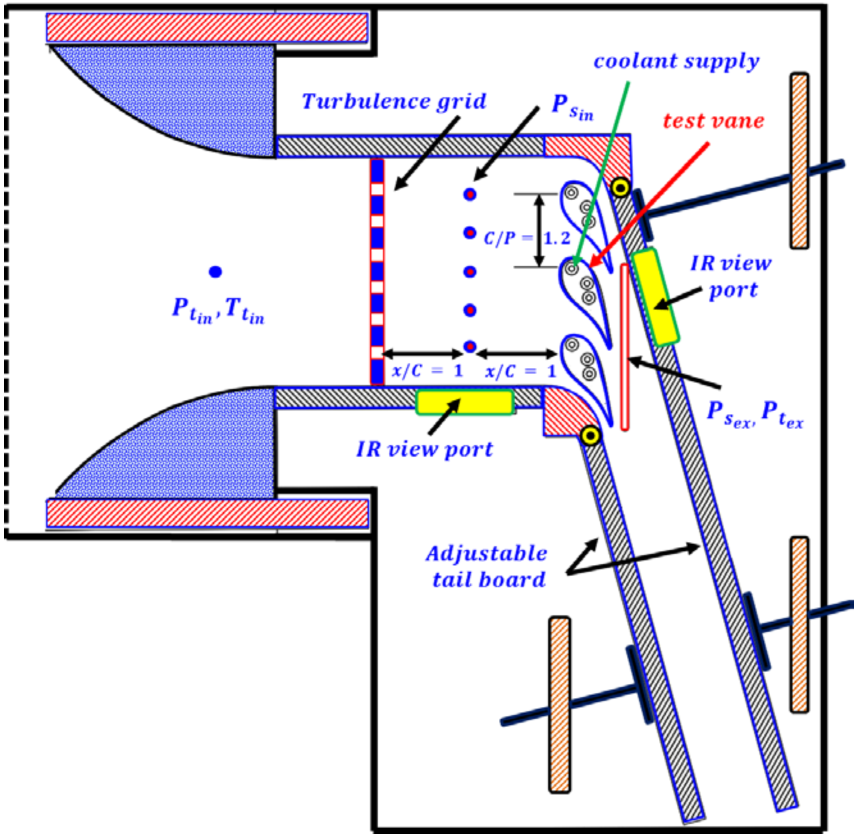

Summary of test conditions

Measurement	Blowing ratio
Film effectiveness	0.25 – 2.23
Convective heat transfer coefficient (HTC)	0.25 – 2.23
Aerodynamic loss	0.95 – 1.85
Discharge coefficient	*Pressure ratio* (1 – 2.2)

Heat Transfer and Film Effectiveness Measurement

- The tunnel can run up to 45 sec at $M_{ex} = 0.8$.
- Surface temperature was measured with a FLIR A325sc infrared camera.

Tunnel temperature response and Mach number

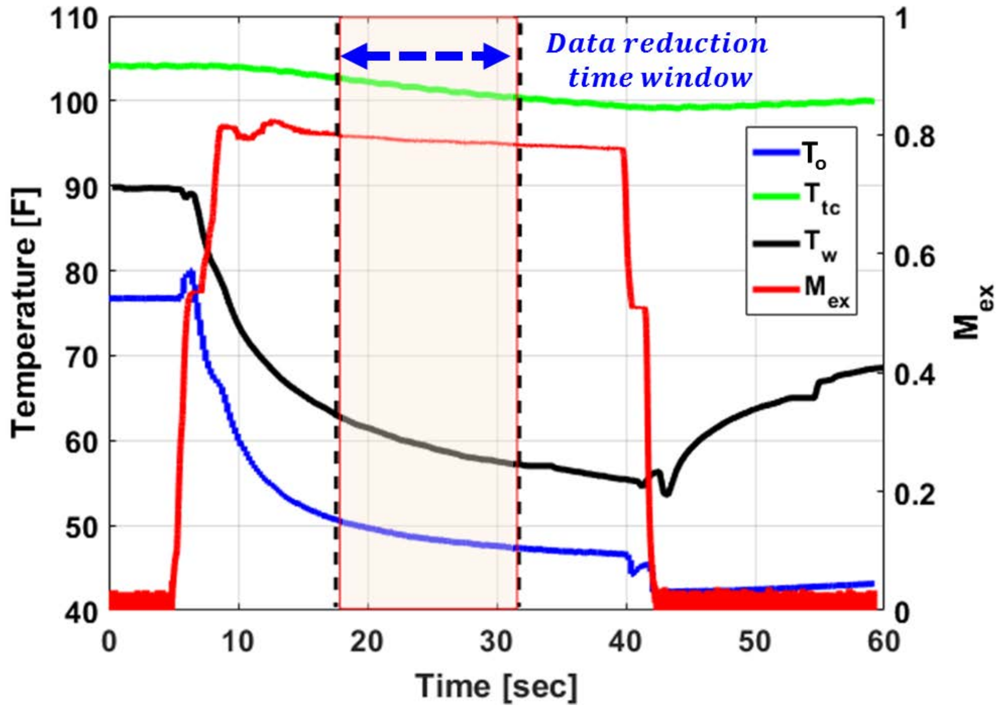

Raw IR image

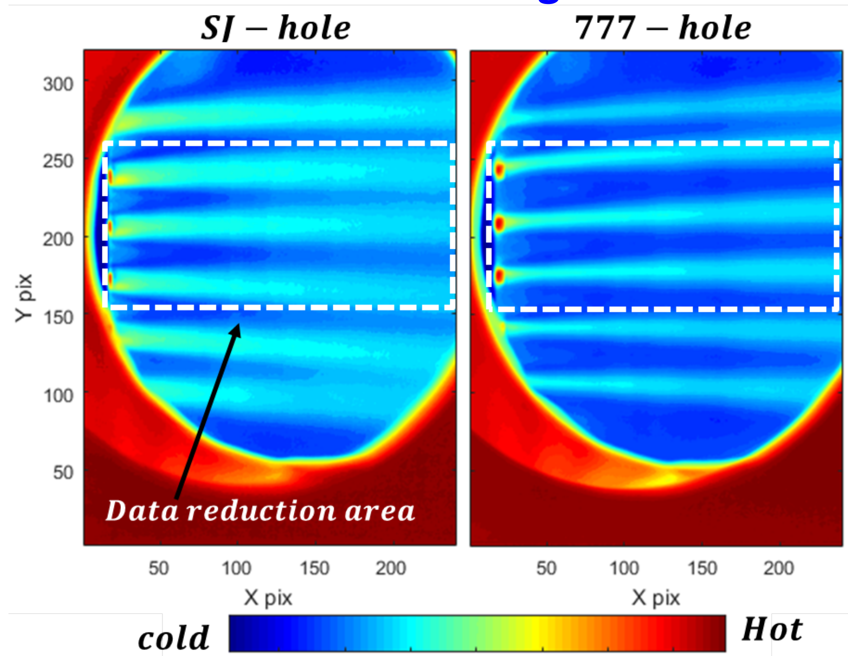

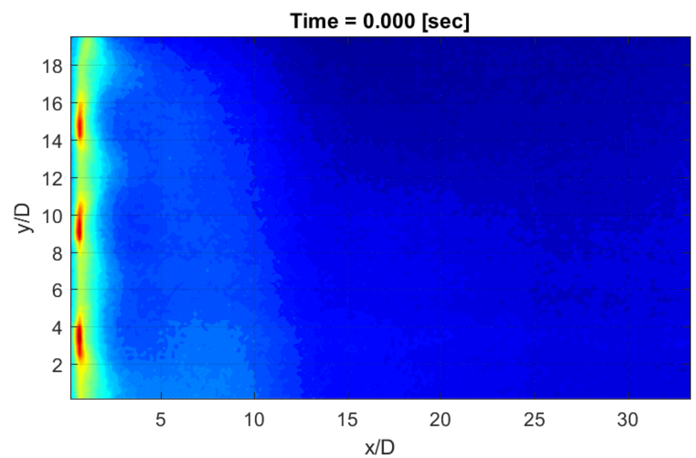

Inverse Heat Transfer Analysis

- A **Dual Linear Regression Technique (DLRT) [Xue et al. 2015]** was used to estimate the film effectiveness and heat transfer coefficient.
- Experiments were performed twice for two different coolant temperature.

$$q(t_m) = \frac{2\cdot\sqrt{k\cdot\rho\cdot c}}{\sqrt{\pi\cdot\Delta t}}\cdot\sum_{i=2}^{m}\frac{T_i - T_{i-1}}{(m-i)^{\frac{1}{2}}+(m-i+1)^{\frac{1}{2}}}$$

(Schultz et al., 1973)

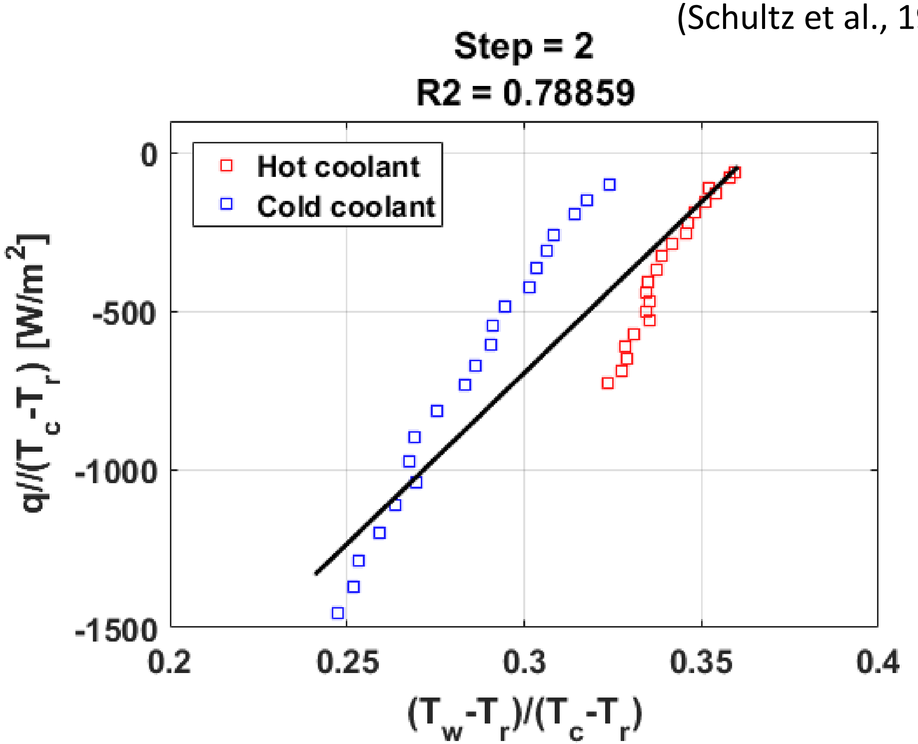

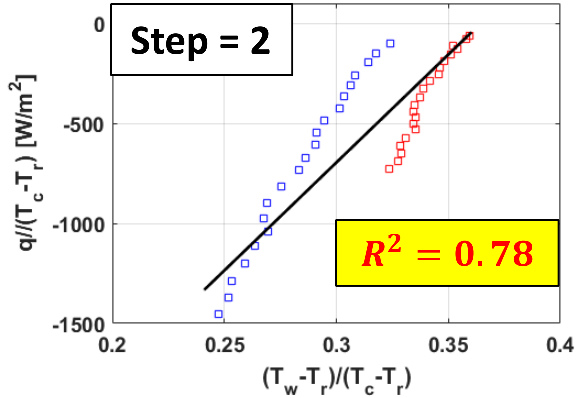

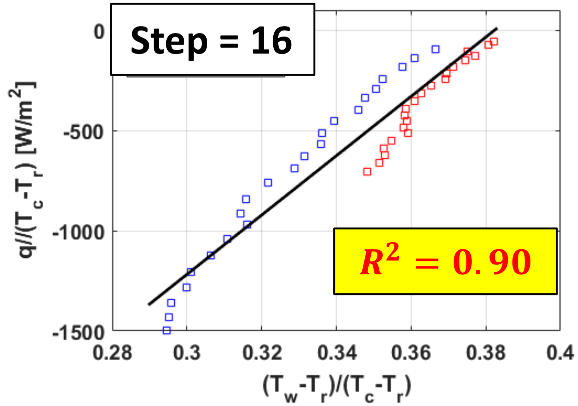

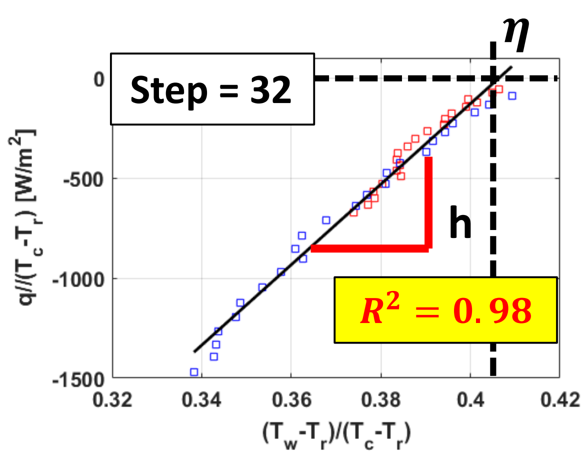

Film Effectiveness (Tu = 0.7%)

- **Strong periodicity** was observed for both SJ and 777-hole.
- A **higher effectiveness** value was observed in the lateral direction for SJ hole compared to 777- hole at **high blowing ratio.**

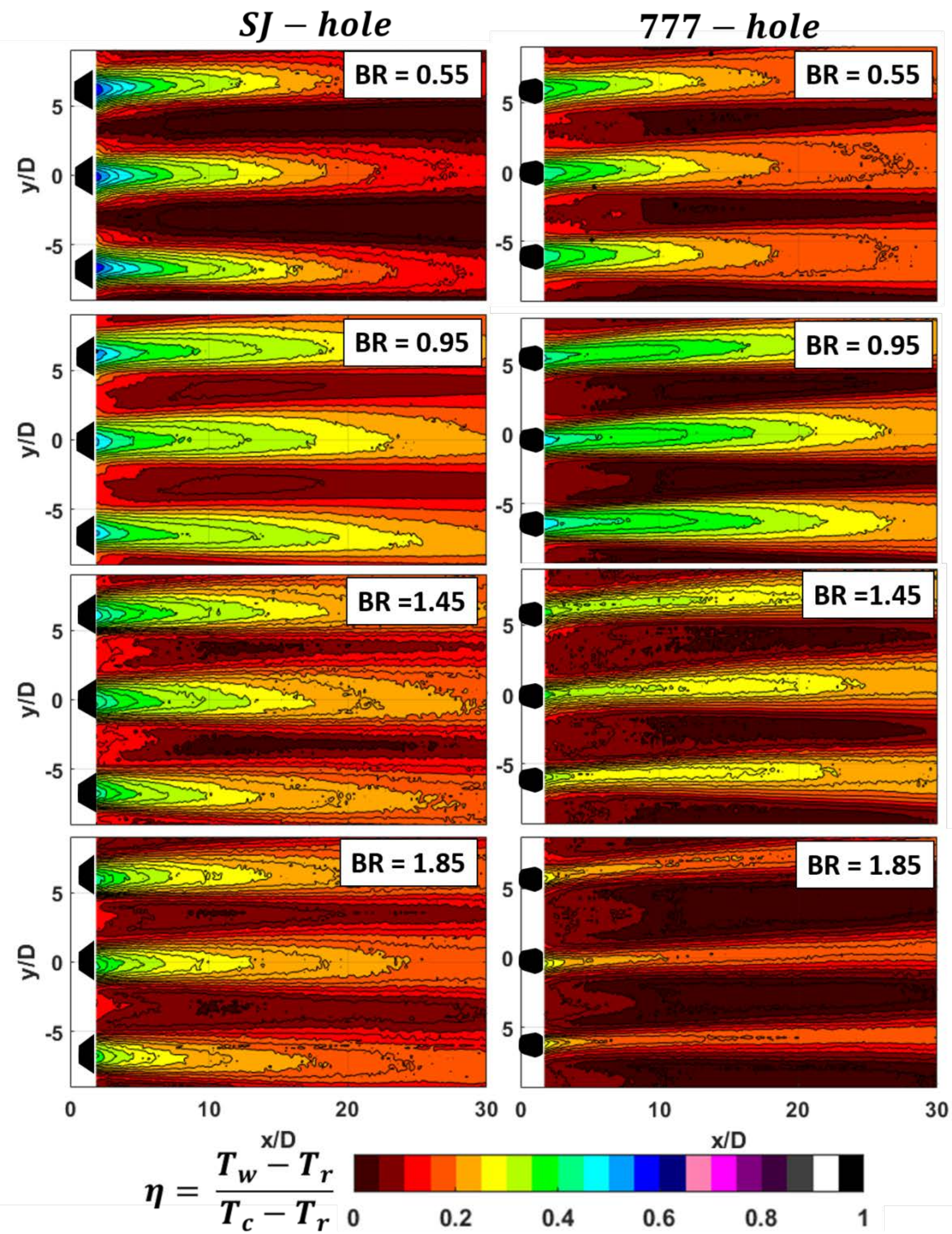

Film Effectiveness (Tu = 6.0%)

- The freestream turbulence increases mixing thus the film effectiveness drops.
- The SJ hole outperformed the shaped hole at high blowing ratios.
- The lateral spreading of the coolant increases with freestream turbulence for 777-hole at BR > 1

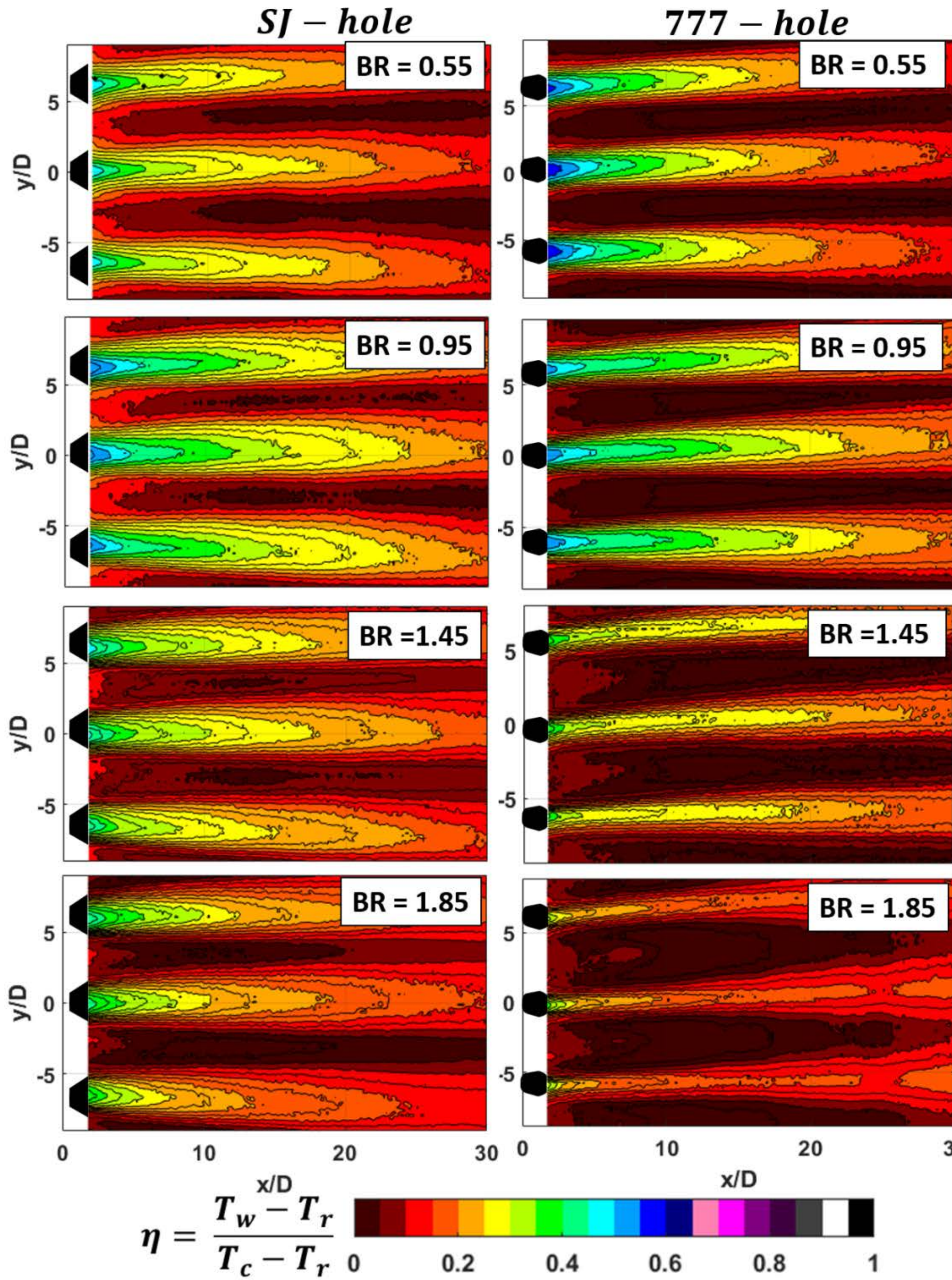

Average Film Effectiveness

- The SJ hole shows higher laterally averaged cooling effectiveness in the near hole region at high blowing ratios (BR > 1).

Area for averaging

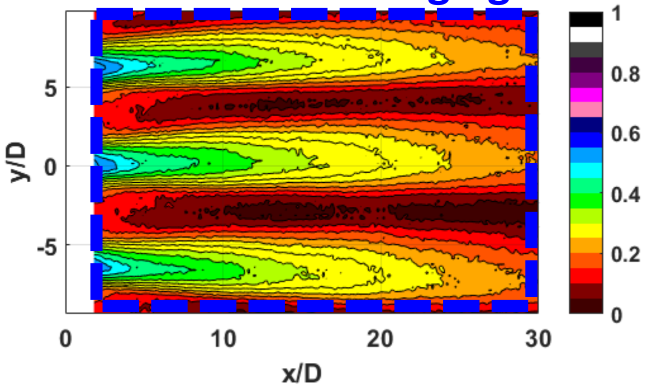

Span averaged effectiveness

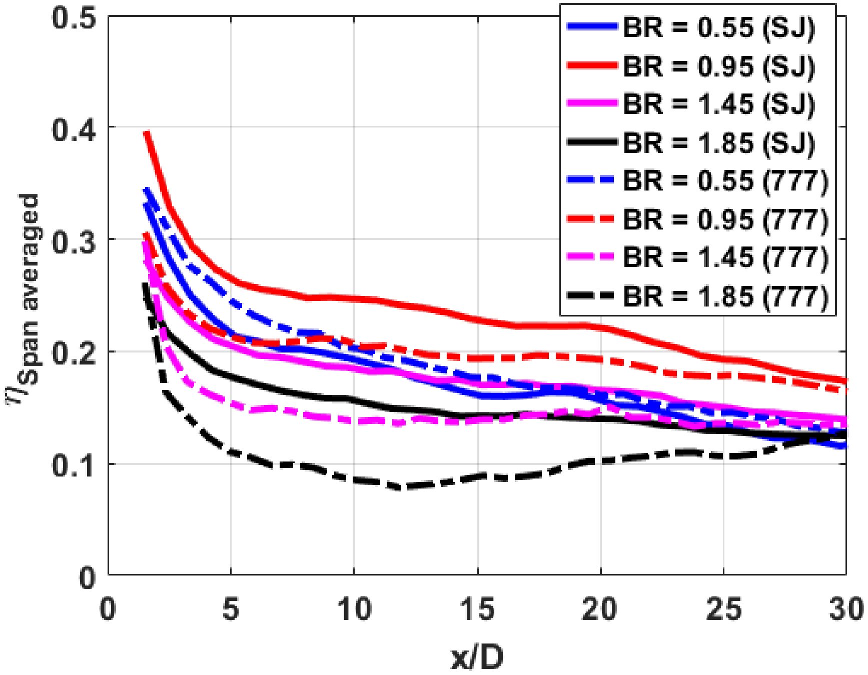

Area averaged effectiveness

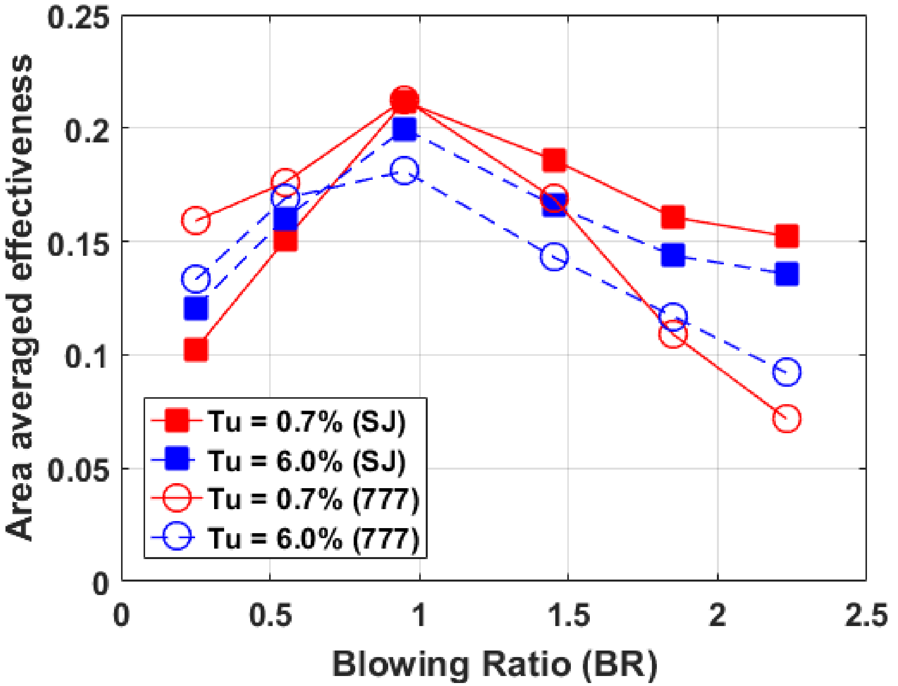

Heat Transfer Augmentation

- Both holes show heat transfer augmentation with increasing blowing ratio.
- Heat transfer augmentation for the SJ hole is higher in the near hole region compared to the 777-shaped hole.

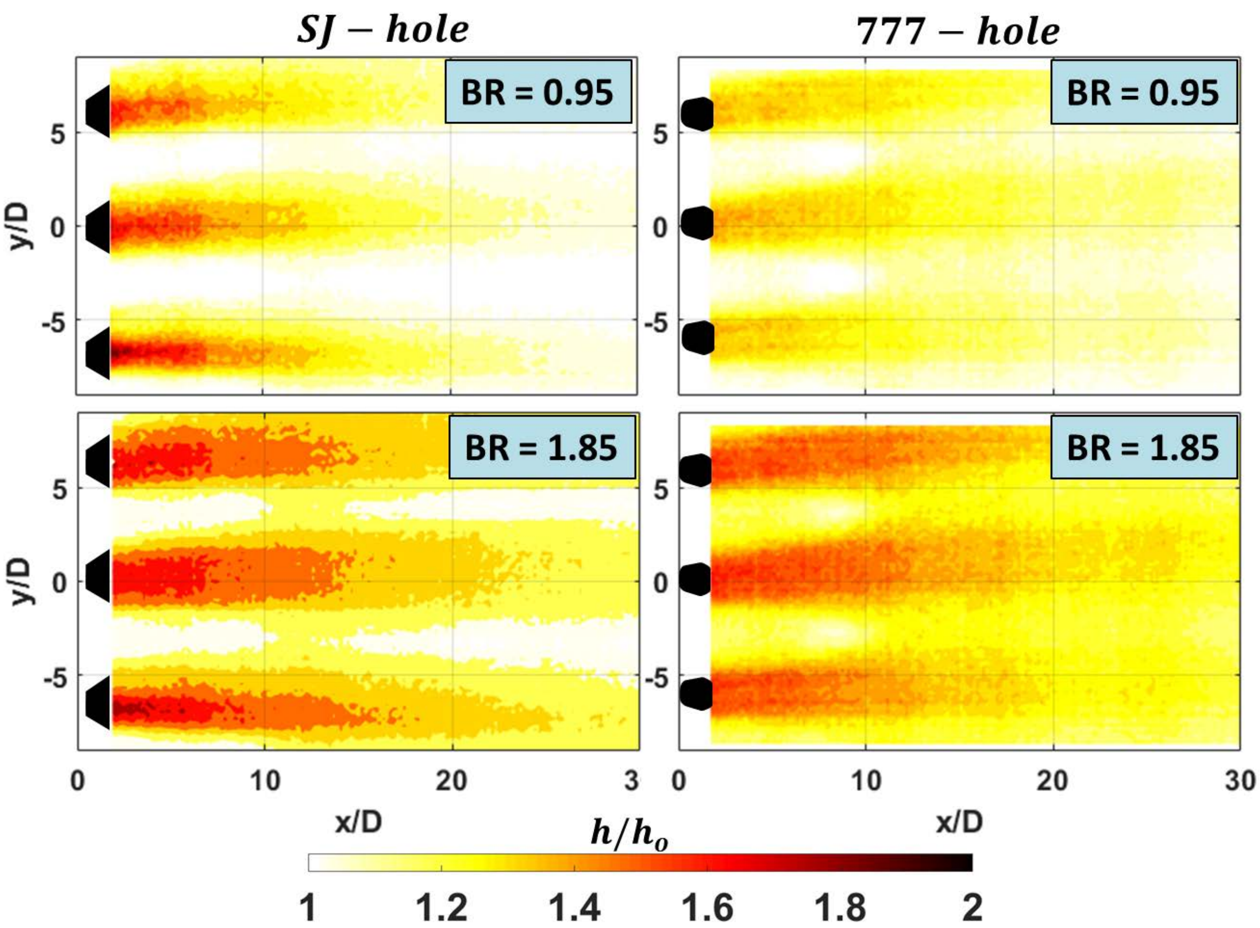

Net Heat Flux

$$\frac{q}{q_o} = \frac{h}{h_o}\left[1 - \eta\,\frac{(T_\infty - T_w)}{(T_\infty - T_c)}\right] = \frac{h}{h_o}\left[1 - \frac{\eta}{\Phi}\right]$$

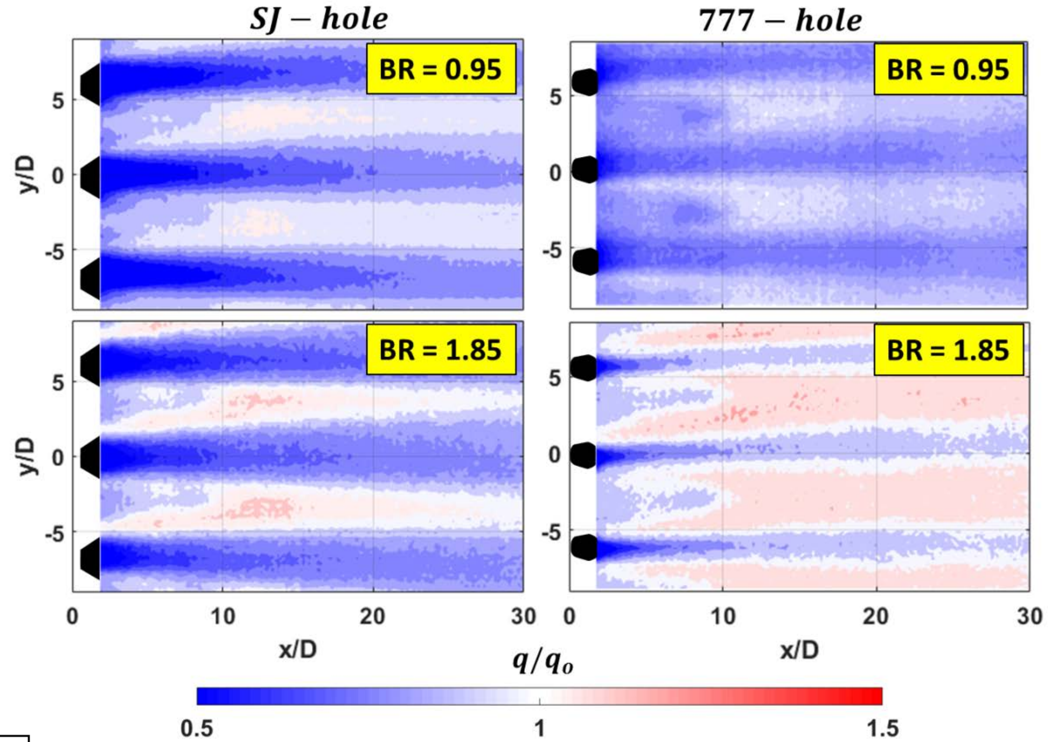

- Heat flux ratio significantly improves for the SJ hole at high blowing ratio.

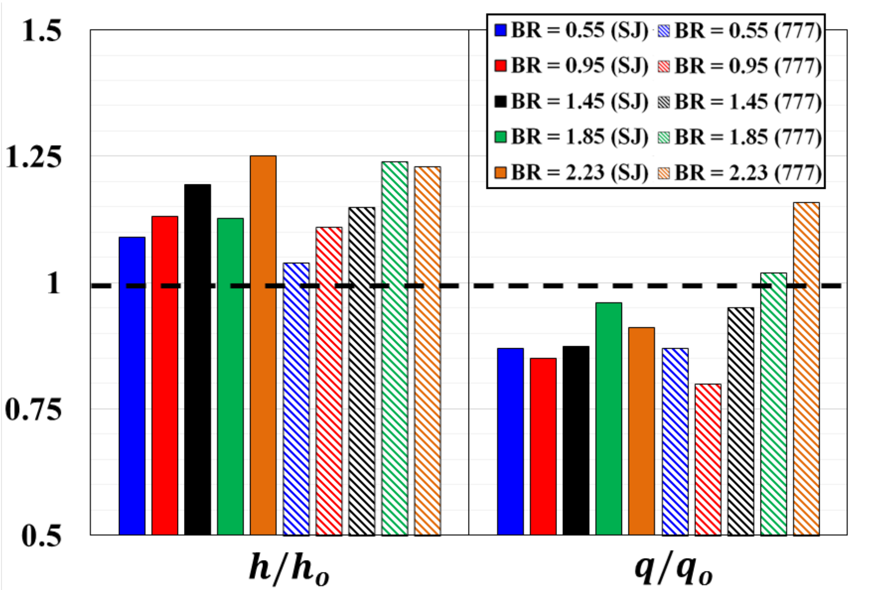

- The sweeping jet hole has a net positive cooling benefit (NPCB) of **15% at M = 0.95** and **10% at M = 2.23**

Trailing Edge Cooling

Background

DMLS relaxes manufacturing constraints. Here are some options that DMLS enables:

- **Near wall cooling passages and center-body:**
  - Narrow cooling passages **close to the walls**.
  - Uncooled center-body **supports the vane structurally**.

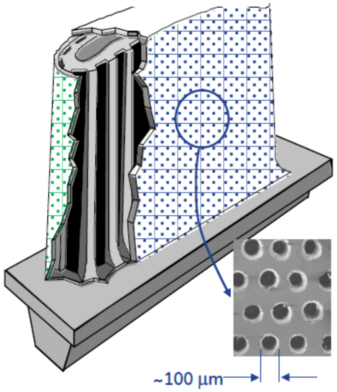

(Bunker, 2006)

- **Pin clearance:**
  - **Partial length pins** (Arora and Abdel-Messeh found 50% drop in pressure loss but negligible affect the heat transfer)

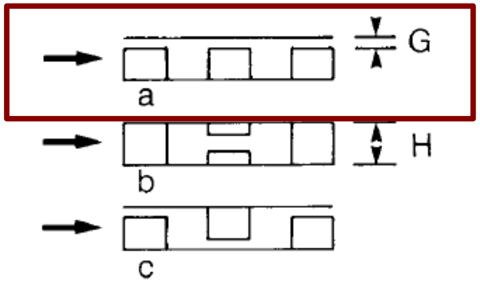

(Arora and Abdel-Messeh, 1990)

- **Pin Shape:**
  - **Triangular pins outperform** circular pins in terms of heat transfer (Ferster et al. (2017)


(Ferster et al., 2017)

Trailing Edge Cooling (Subsonic Study)

- heat transfer performance and pressure drop
- low speed linear cascade
- pin fin with clearance and a center-body (PFC) and conventional pin fin (PF)
- S/D=2, X/D=1, H/D=[1.25,8.87] for PF and [0.9, 2.25] for PFC
- 17 full pin rows (PF); PFC has 5 full and 12(ps) and 13(sc) partial pin rows
- Partial pins had 23% gap to channel height ratio
- Two different freestream turbulence intensity (Tu=14% and 6%)
- Two different cold flow mass flow rates ($\dot{m} = 4.44$ *and* $6.41\ g/s$)

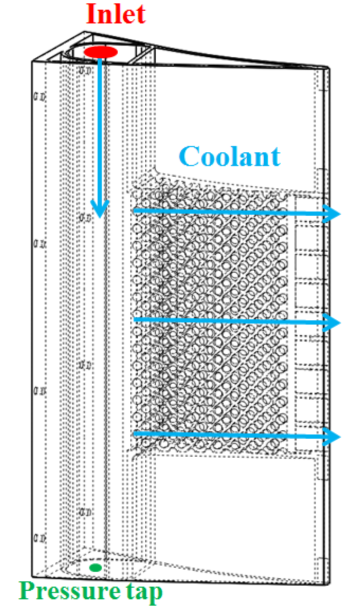

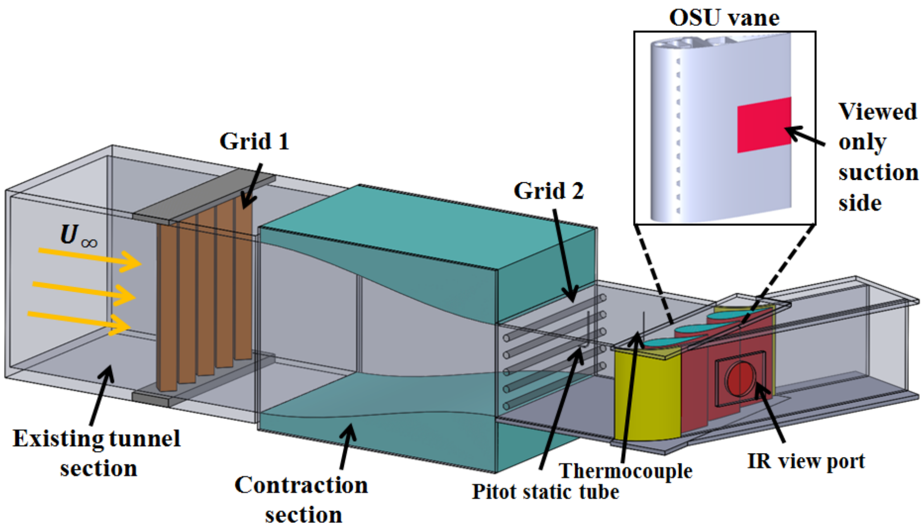

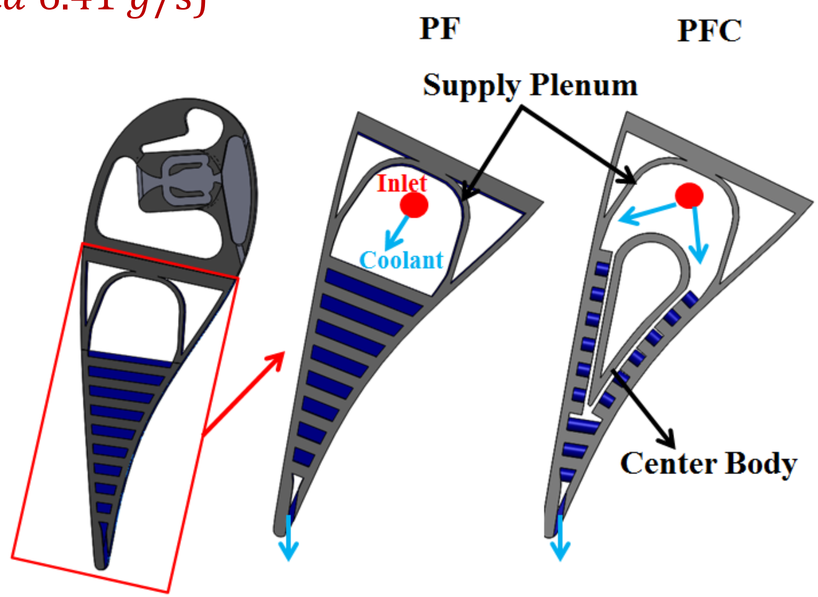

Trailing Edge Cooling (Heat transfer result)

Overall Cooling Effectiveness (Φ)

$$\Phi = \frac{T_{ad} - T_w}{T_{ad} - T_{c,i}}$$

T_{ad} =Adiabatic wall temperature
T_w= Steady state wall temperature
$T_{c,i}$ = Coolant temperature at the supply plenum

	Nominal Test Conditions	Uncertainty
U_∞	10 m/s	±0.25 m/s
T_∞	100-108 °F	±0.5°F
$T_{c,i}$	60-68 °F	±0.5°F
$\dot{m}$	4.44-6.41 g/s	±0.17-0.18 g/s
$\bar{\Phi}$	0.1711	±0.044

- The PFC design shows a much more **uniform effectiveness** between x/C=0 and 0.3 compared to the PF design. This is largely because of the variation in the **internal cooling channel cross sectional area.**

Less thermal stress for PFC than PF

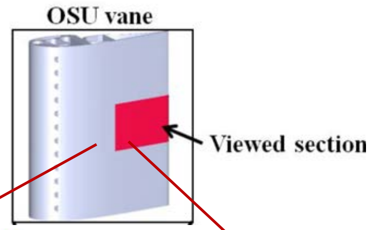

IR view includes only 5 out of 9 ejection slots.

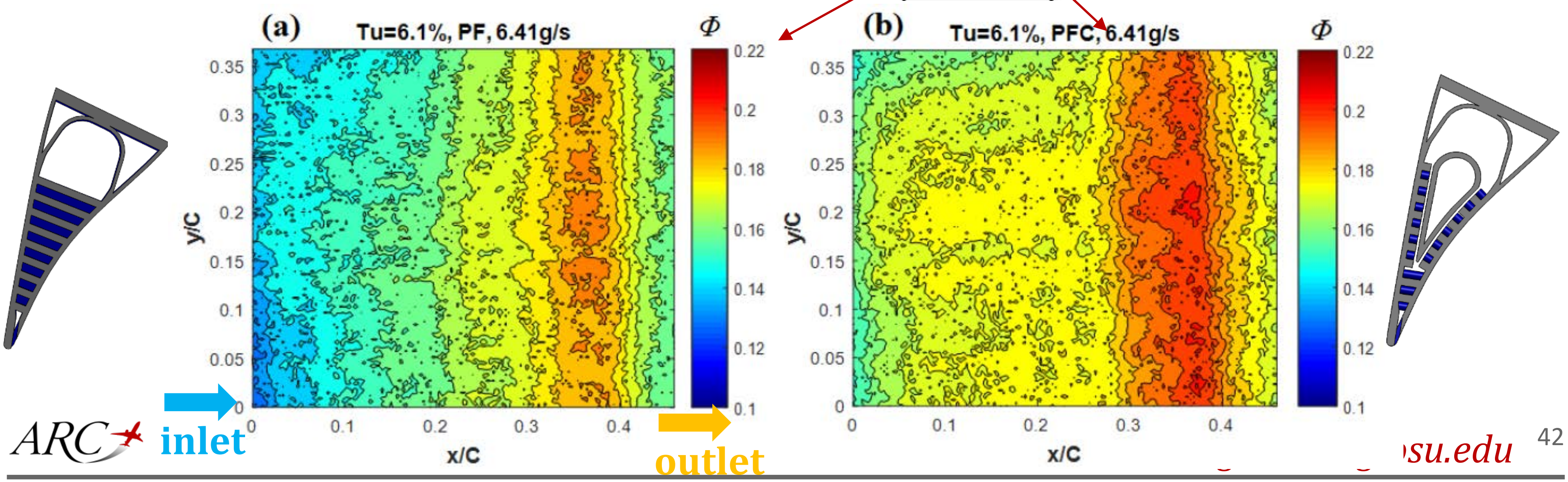

Trailing Edge Cooling (Heat transfer result)

The Effect of Cooling Design on Span Averaged Overall Cooling Effectiveness

- Partial pins with clearance in the PFC design shows **~6% (high Tu) and ~13% (low Tu)** higher span averaged cooling effectiveness due to higher coolant velocity than the PF design as a result of **reduced flow area.**

- The full pin and ejection slot portion of PFC creates **similar span averaged overall effectiveness** with the corresponding location in PF due to the **similar geometric configuration.**

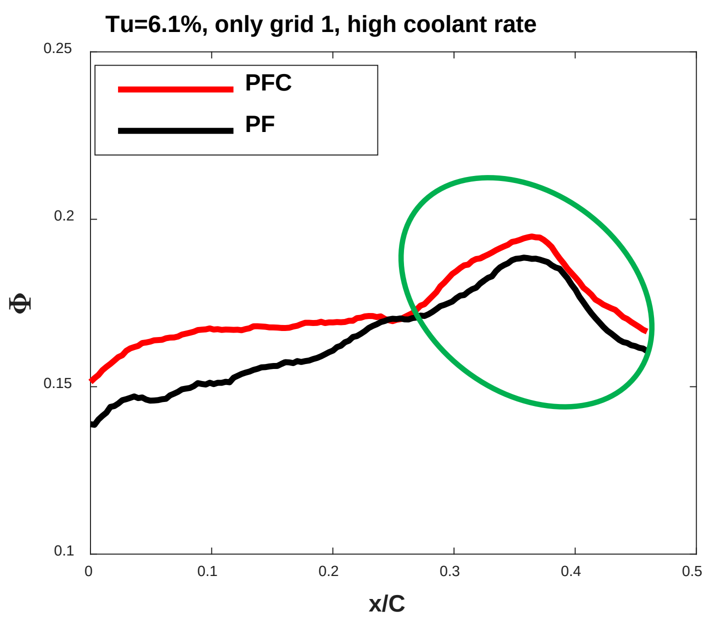

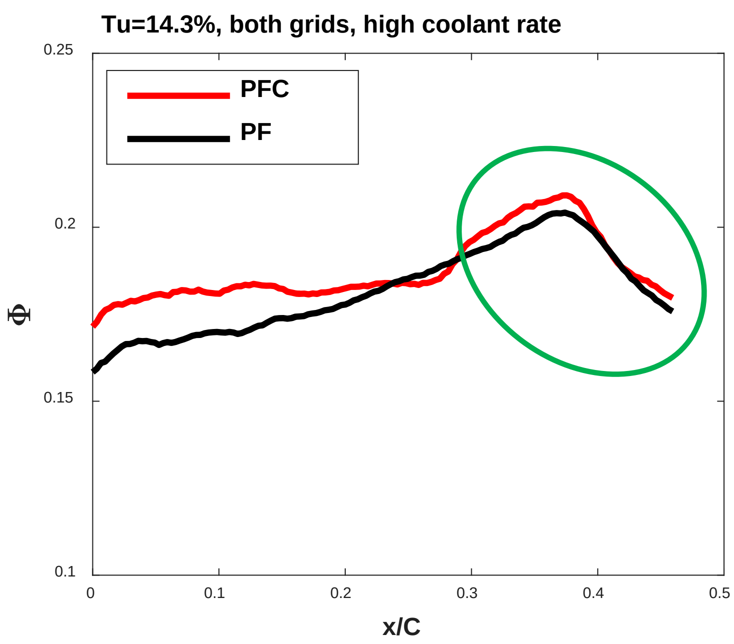

Trailing Edge Cooling (Heat transfer result)

Area Averaged Overall Cooling Effectiveness ($\bar{\Phi}$)

- Φ was area averaged over **the full IR view field**.

- At low Tu, PFC shows **~6% higher $\bar{\Phi}$ than the PF design**.
- At high Tu, PFC shows **~2.5% higher $\bar{\Phi}$ than PF**.

- Due to the **highly cooled regions** where the pins have **clearance and center-body is present .**

- **For comparable cooling effectiveness, 15% less massflow with PFC**

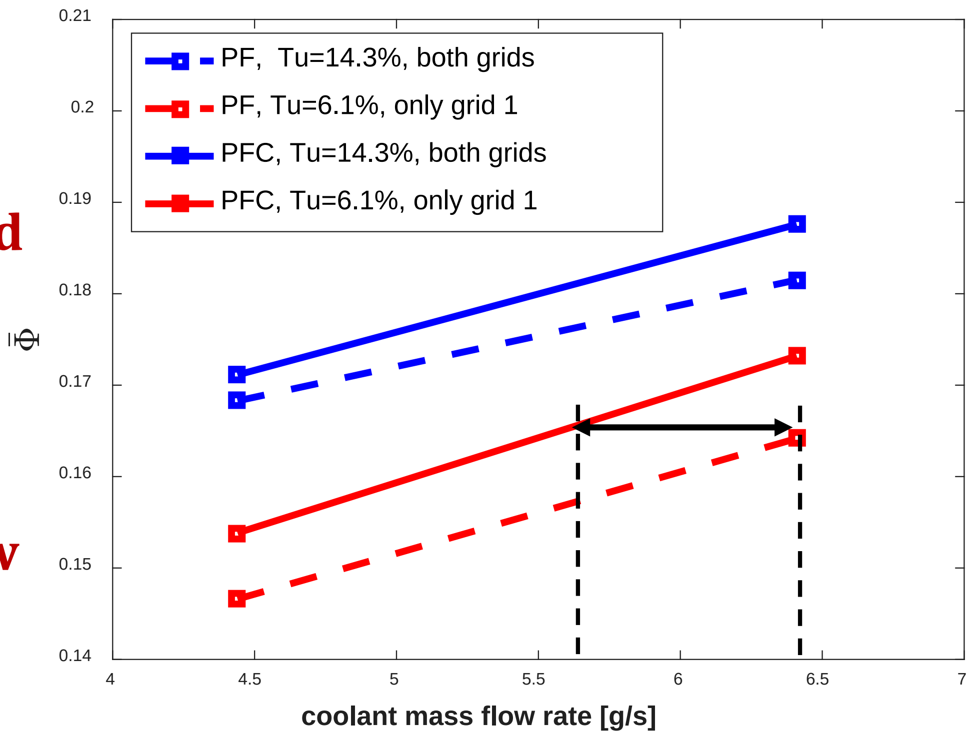

Trailing Edge Cooling (Pressure drop)

- PFC and PF geometries generate **similar pressure ratios** for the studied mass flow rates.
- The similarity in pressure drop between PF and PFC geometries was expected, and is the result of **two counteracting effects**.

Case 1 → Case 2	**Case 2 → Case 3**
pressure drop decreases due to flow area increases	*pressure drop increases due to flow area decreases*

- ΔP = Pressure drop across the test piece
- P_{atm} = Atmospheric pressure
- P_{in} = Pressure of the supply plenum

$$P_{in} = P_{atm} + \Delta P$$

PF to PFC

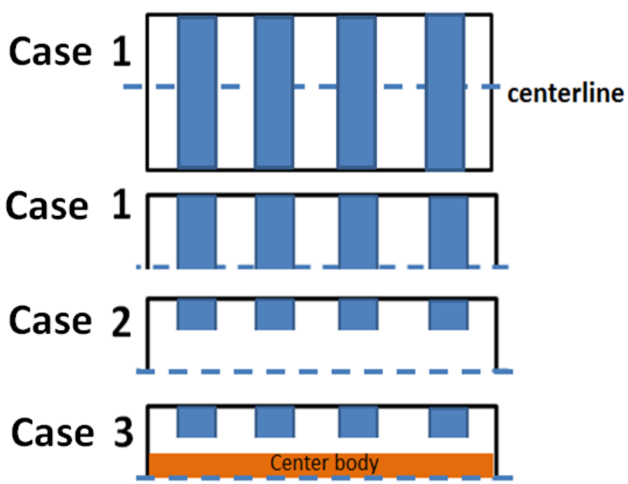

Pressure Ratio

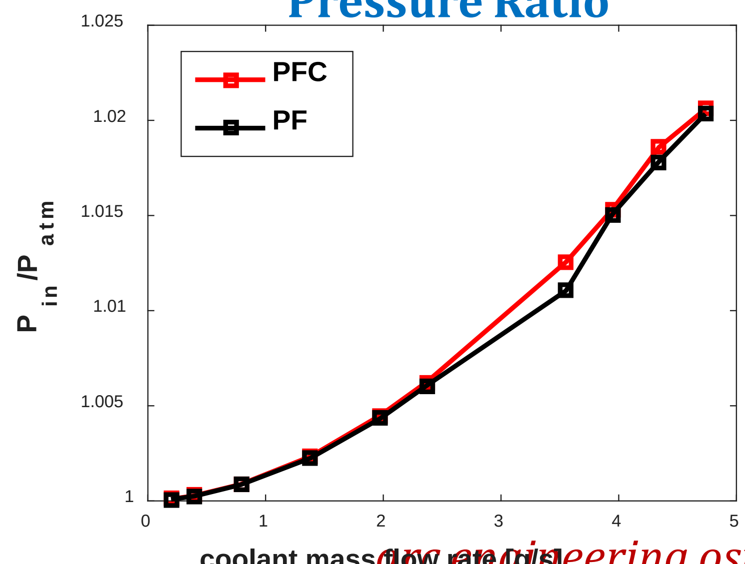

Trailing Edge Cooling (Transonic TE Study)

- Small scale PF and PFC designs were printed for transonic cascade experiments.
- After heat transfer tests, PFC developed a bump in the region where pins do not touch the center body (partial length pins).
- Some of the partial pins were converted to full pins to strengthen the walls.

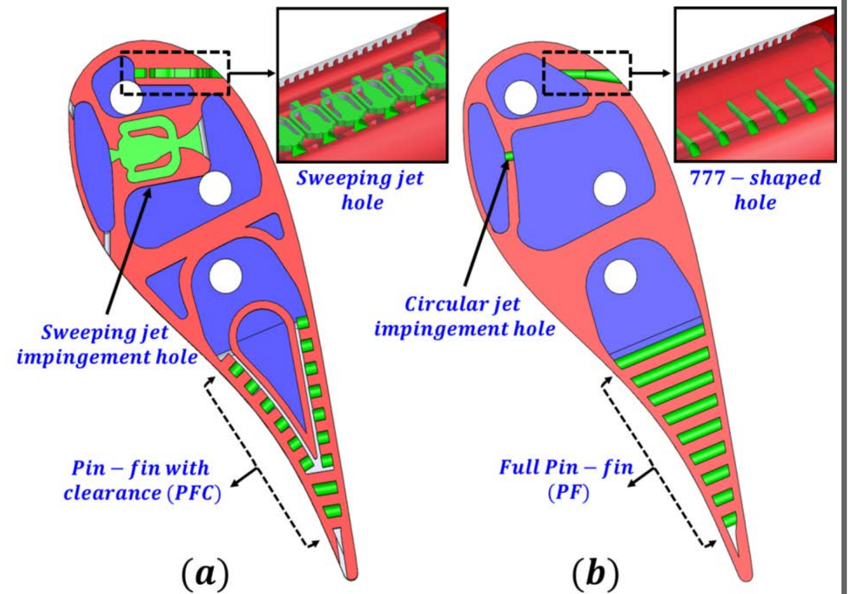

(a) Initial PFC and (b) PF design

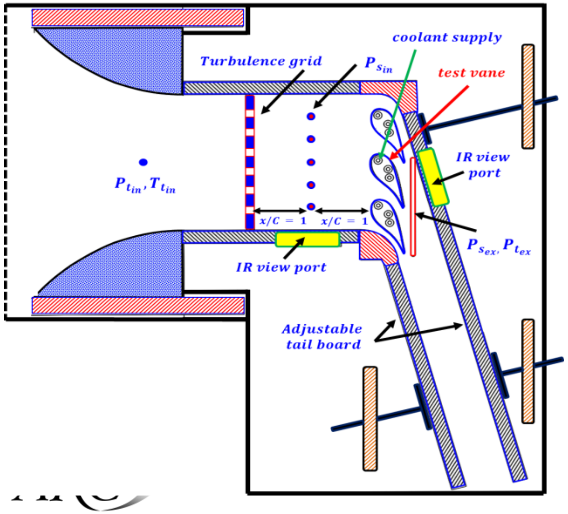

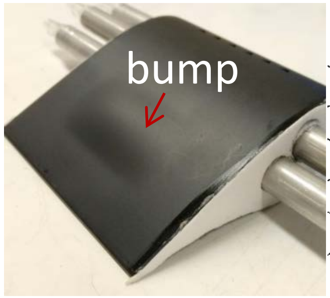

Initial PFC design

Partial length pins

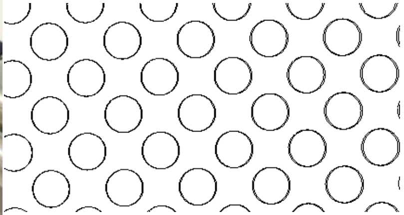

Modified PFC design

Full and partial length pins

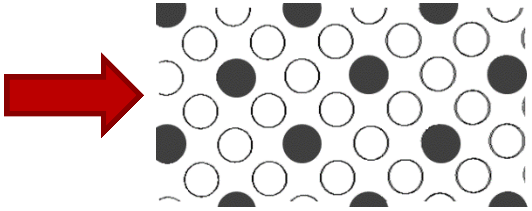

Trailing Edge Cooling (Heat Transfer experiment)

- Coolant was supplied from **two sides** in span-wise direction.
- Heat transfer tests were done for various coolant mass flow rates with **hot** and **cold coolant** which were were **hotter than the freestream temperature.**

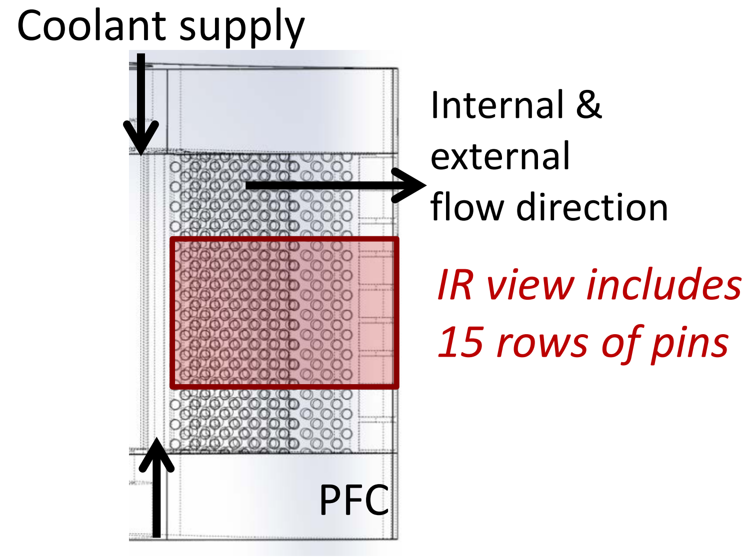

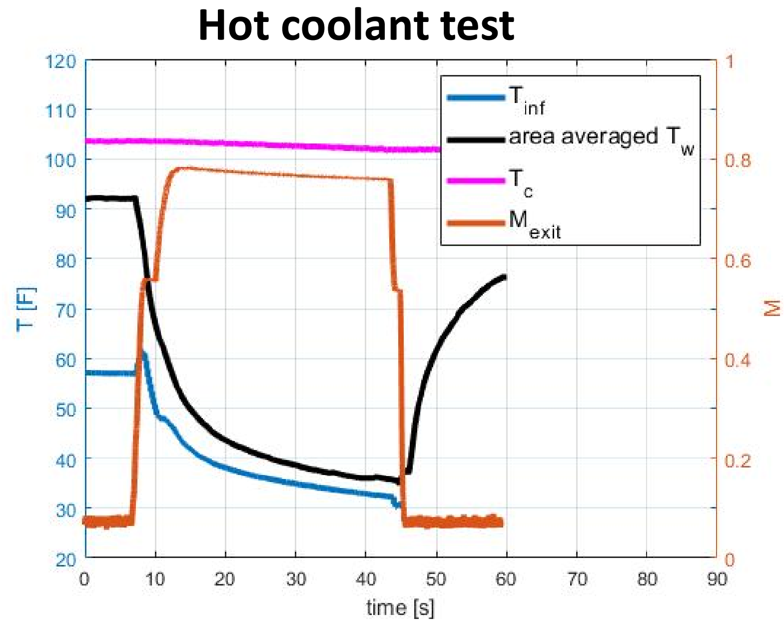

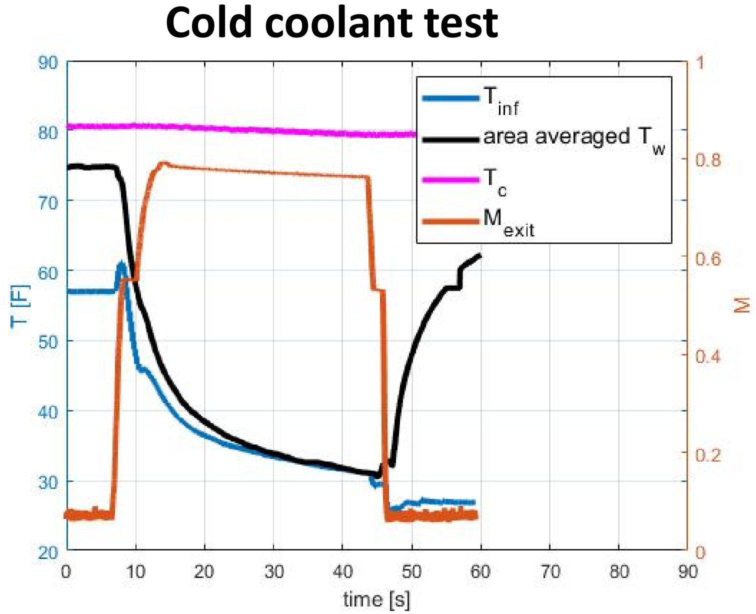

Trailing Edge Cooling (Heat Transfer experiment)

- **Overall cooling effectiveness (Φ)** was utilized to compare heat transfer performances of the two designs.

$$\Phi = \frac{T_w - T_r}{T_{c,i} - T_r}$$

- **Transient wall temperature (T_w)** was measured by IR camera.

- **Recovery temperature (T_r)** is the reference temperature that corresponds to the same Φ values of hot and cold coolant cases for a mass coolant rate. T_r was calculated for each pixel.

$$\Phi = \frac{T_{w,hot} - T_r}{T_{c,hot} - T_r} = \frac{T_{w,cold} - T_r}{T_{c,cold} - T_r}$$

- **Coolant temperature at the supply plenum ($T_{c,i}$)** was measured at the mid-span in the supply plenum.

Trailing Edge Cooling (Heat Transfer result)

The Effect of Freestream Turbulence on Span Averaged Cooling Effectiveness

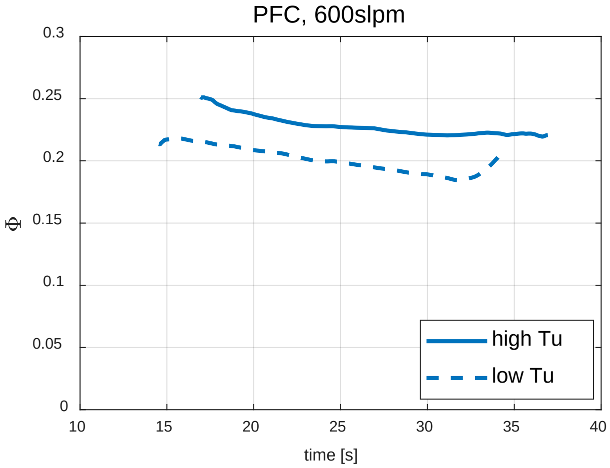

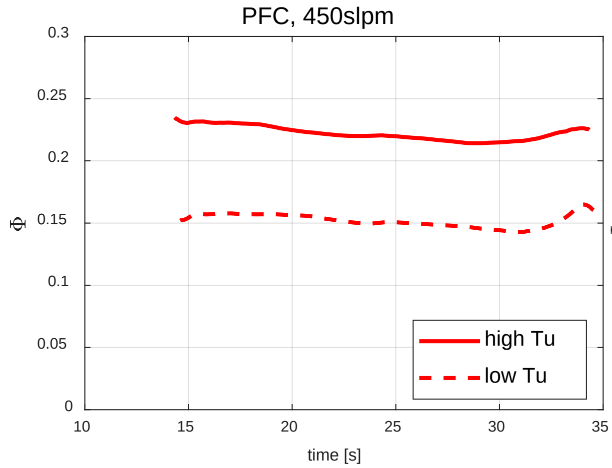

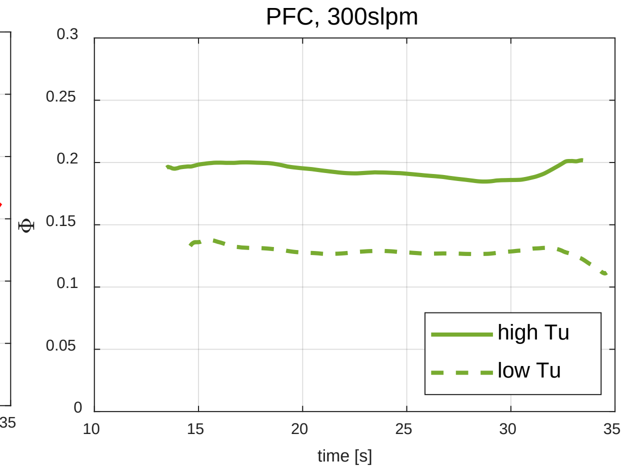

The Effect of Cooling Design on Span Averaged Overall Cooling Effectiveness

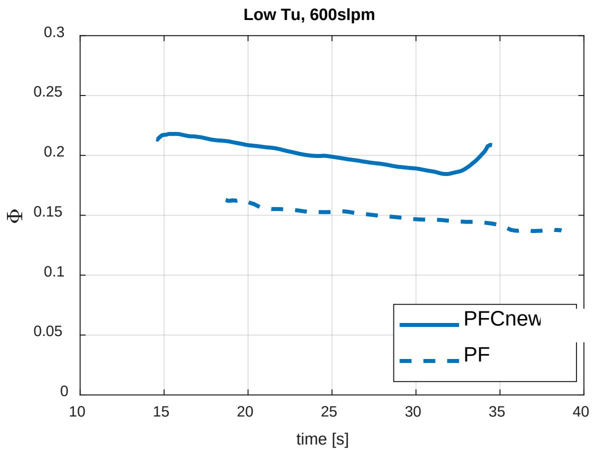

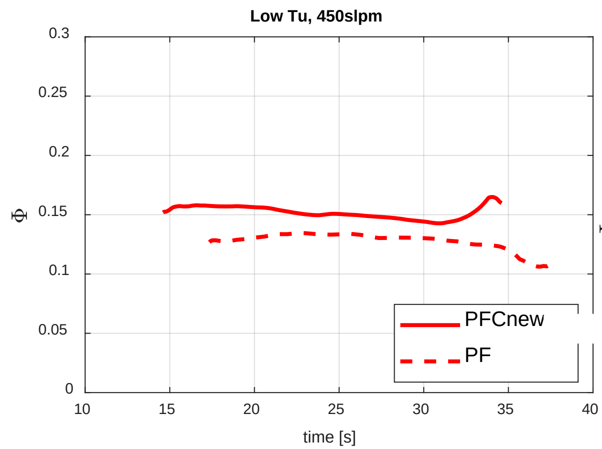

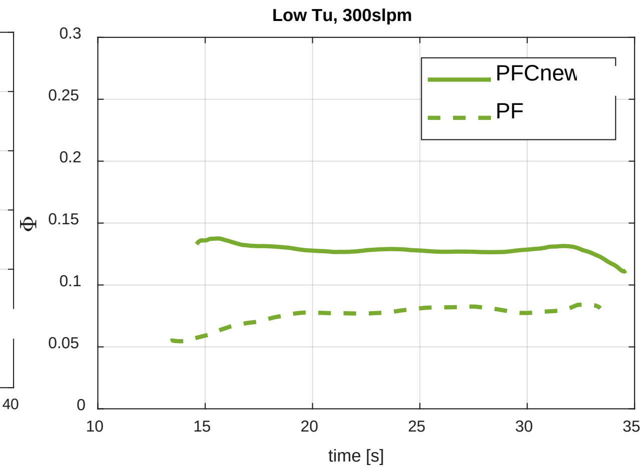

Trailing Edge Cooling (Heat Transfer result)

- Time average was done in between 20s and 30s.
- Area average was performed over the whole IR view field.

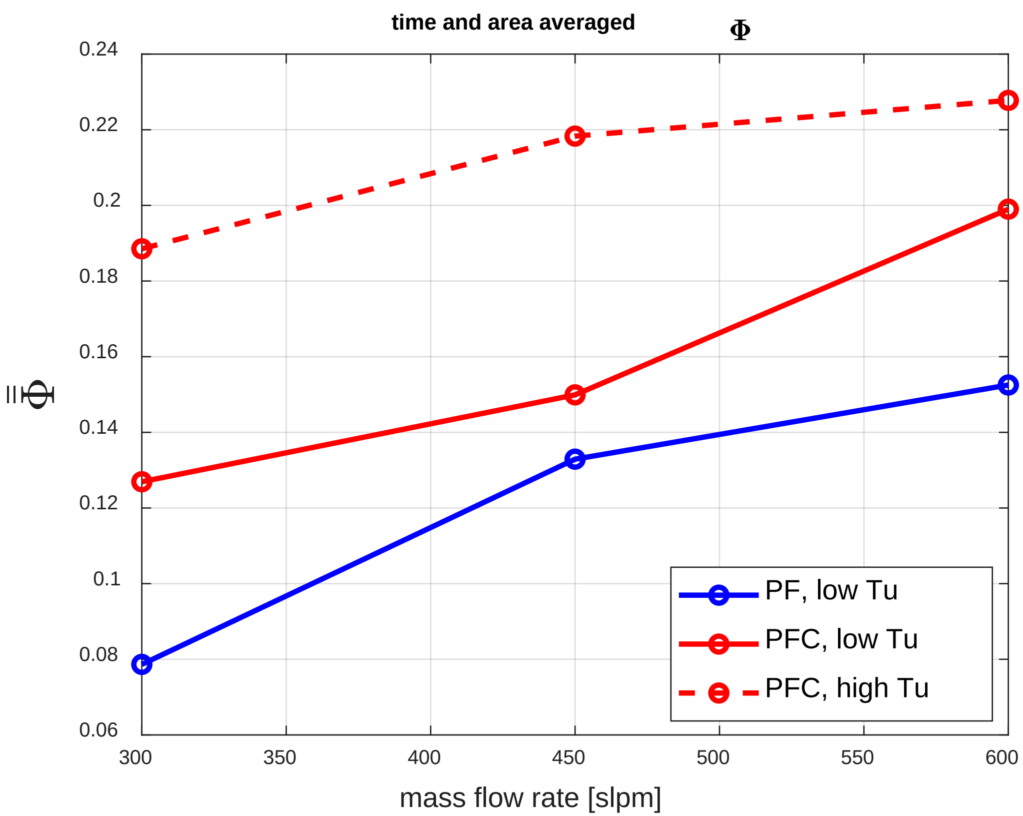

Sweeping Jet Impingement Cooling

Design Variables

- **Effect of Curvature**
- **Exit fan angle of the nozzle**

Effect of Curvature (Curvature Configuration)

- Three different surface curvature configurations are studied –
  - **Case A**: Flat surface ($\boldsymbol{R} = \infty$)
  - **Case B**: Moderate curvature ($\boldsymbol{R = 20D_h}$)
  - **Case C**: High curvature ($\boldsymbol{R = 10D_h}$)

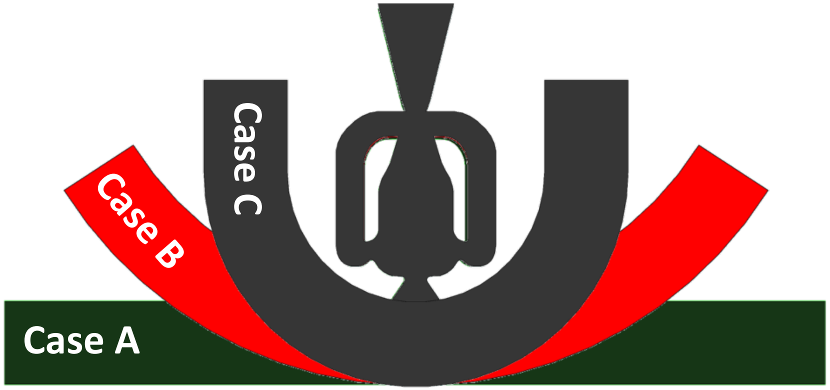

Steady jet

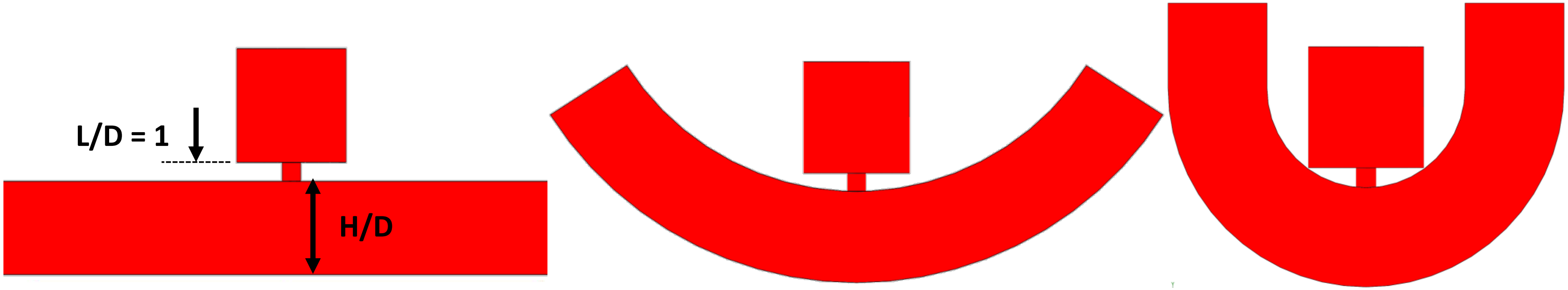

Case D
Flat surface
($R = \infty$)

Case E
Moderate curvature
($R = 20D_h$)

Case F
High curvature
($R = 10D_h$)

Effect of Curvature (Computational model)

- Unsteady RANS **(3D-URANS)** simulation.
- Platform: FLUENT
- Spatial discretization: second order upwind scheme.
- Temporal discretization: second order implicit.
- Turbulence model: $k-\omega\ SST$ model
- Inlet condition: massflow inlet
- Inlet turbulence intensity: 0.4%
- Inlet length scale: 0.0065m.
- Outlet condition: pressure outlet (ambient).
- Target wall: constant heat flux.

$$\boxed{q'' = h(T_w - \boldsymbol{T_{ref}})}$$

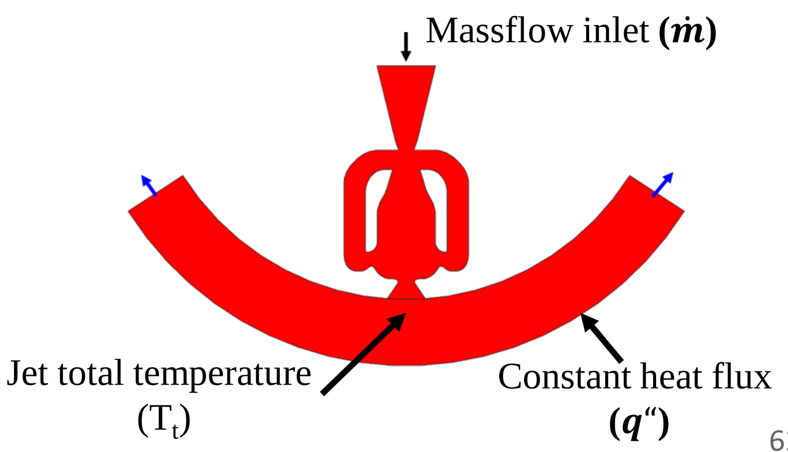

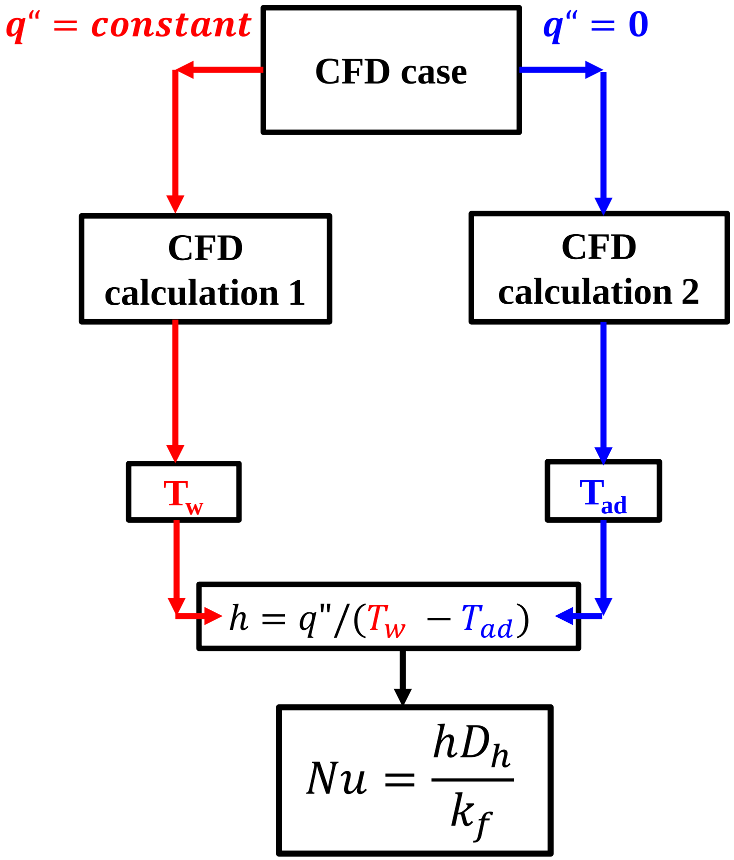

Effect of Curvature (Time averaged Nu)

- Sweeping jet Nu contour shows better uniformity compared to steady jet.
- The effect of surface curvature on sweeping jet local Nu is non-monotonic.

$Re_D = 35,200$ and H/D = 5

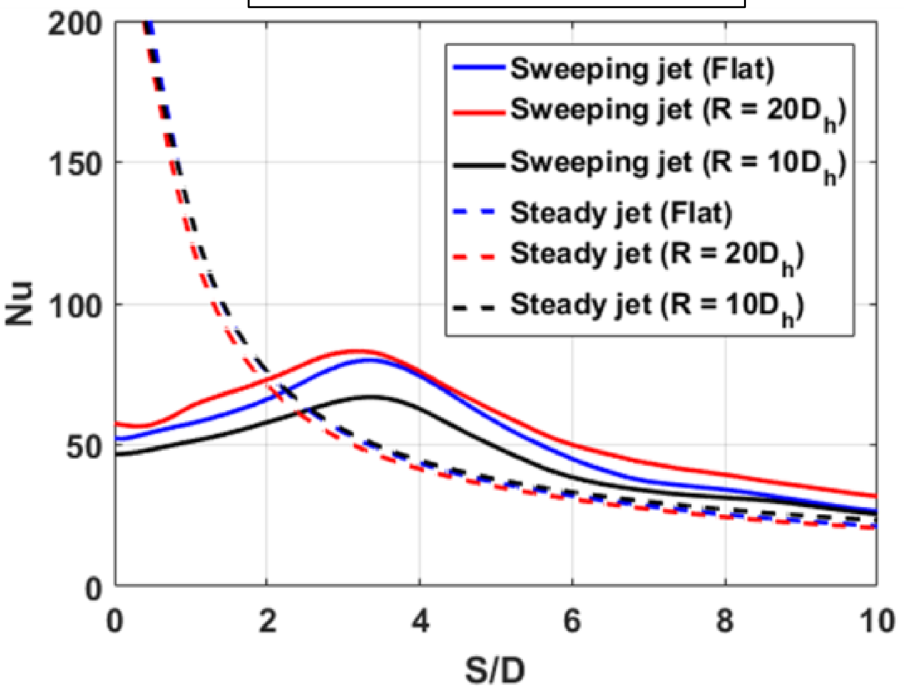

$Nu\ at\ Re_D = 35,200$ and H/D = 5

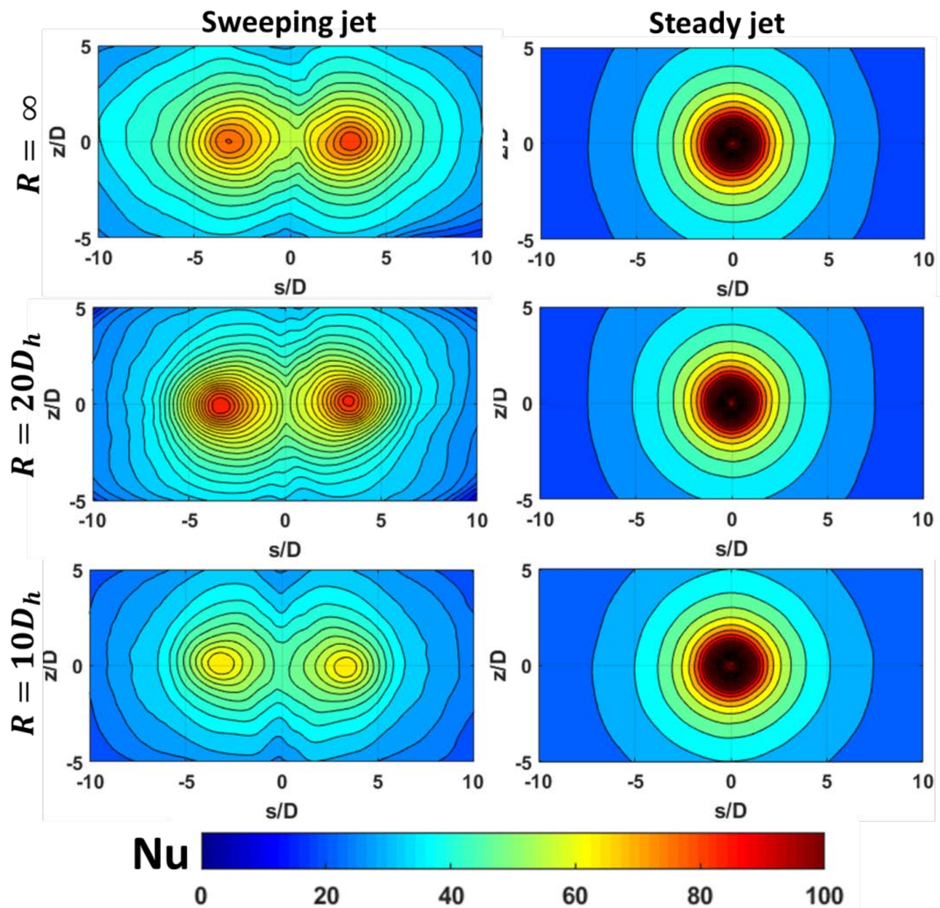

Effect of Curvature (Average Nu)

- Data are averaged over $\pm 10D_h$ in the sweeping direction (axis of oscillation) and $\pm 5D_h$ in the span wise direction.
- The highest Nu_{avg} for sweeping jet tends to be found at moderate curvature ($R = 20D_h$).
- Sweeping jet shows higher Nu_{avg} at H/D = 5 and $R = \infty, 20D$ compared to steady jet.

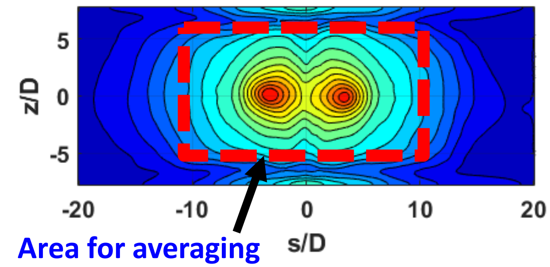

$$h_{avg} = \frac{1}{A}\iint h(s,z)\, dsdz$$

$$Nu_{avg} = \frac{h_{avg} D_h}{K_f}$$

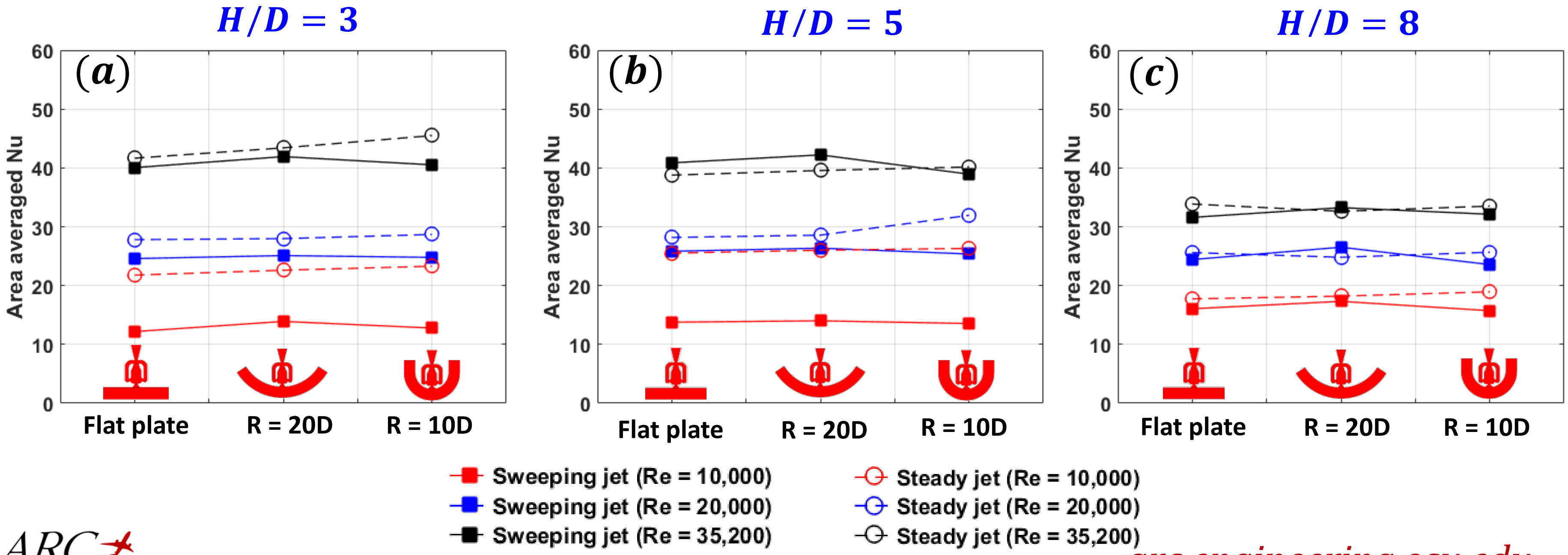

Effect of Curvature (Cooling Uniformity)

- In order to show the actual benefit of the sweeping action, a new parameter has been defined as '**Surface Uniformity Index (γ)**'.

$$\gamma = 1 - \frac{\sum_{i=1}^{N} \sqrt{\left(Nu_i - Nu_{avg}\right)^2}\, A_i}{Nu_{avg}\, A}$$

- $\boldsymbol{\gamma = 1}$ indicates a perfectly uniform surface temperature.

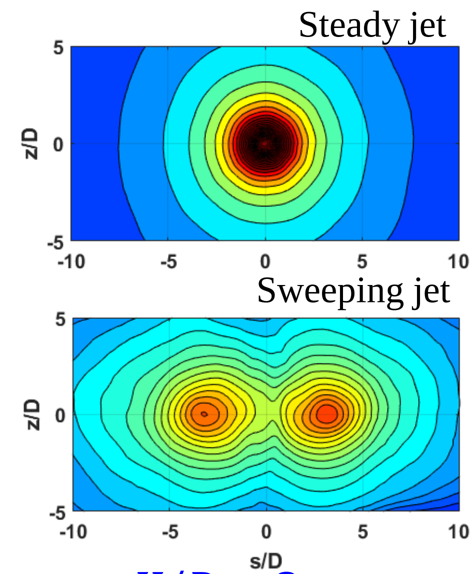

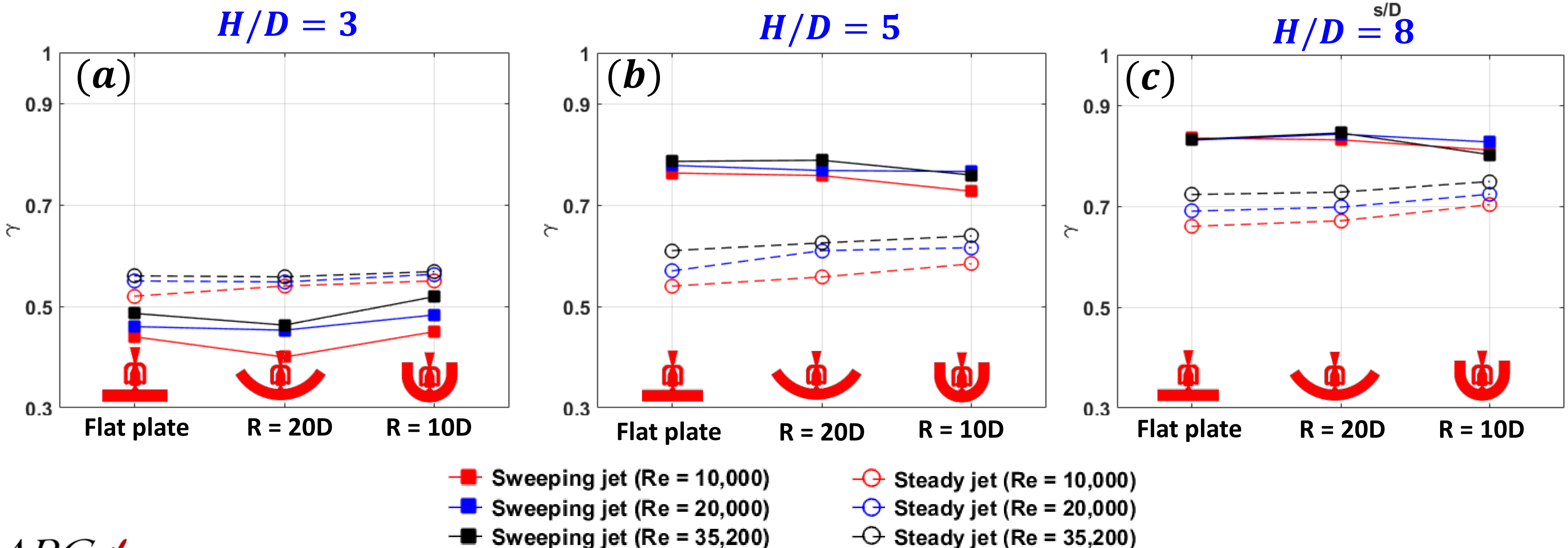

Effect of Exit Fan Angle (Geometry configuration)

- Eight different exit fan angle configurations were studied.
- Throat hydraulic diameter, D = 4.1mm
- Wall-attachment type with an aspect ratio (AR) = 1

Parameter	Value
Exit fan angle ($\boldsymbol{\theta}$)	$0^{\circ}, 20^{\circ}, 40^{\circ}, 55^{\circ}, 70^{\circ}, 85^{\circ}, 100^{\circ}, 130^{\circ}$
Jet to wall spacing ($\boldsymbol{H/D}$)	3, 5, 8
Coolant massflow rate ($\dot{\boldsymbol{m}}_{\boldsymbol{c}}$)	50, 75, 100 slpm
Reynolds number ($\boldsymbol{Re}$)	17000 – 34000

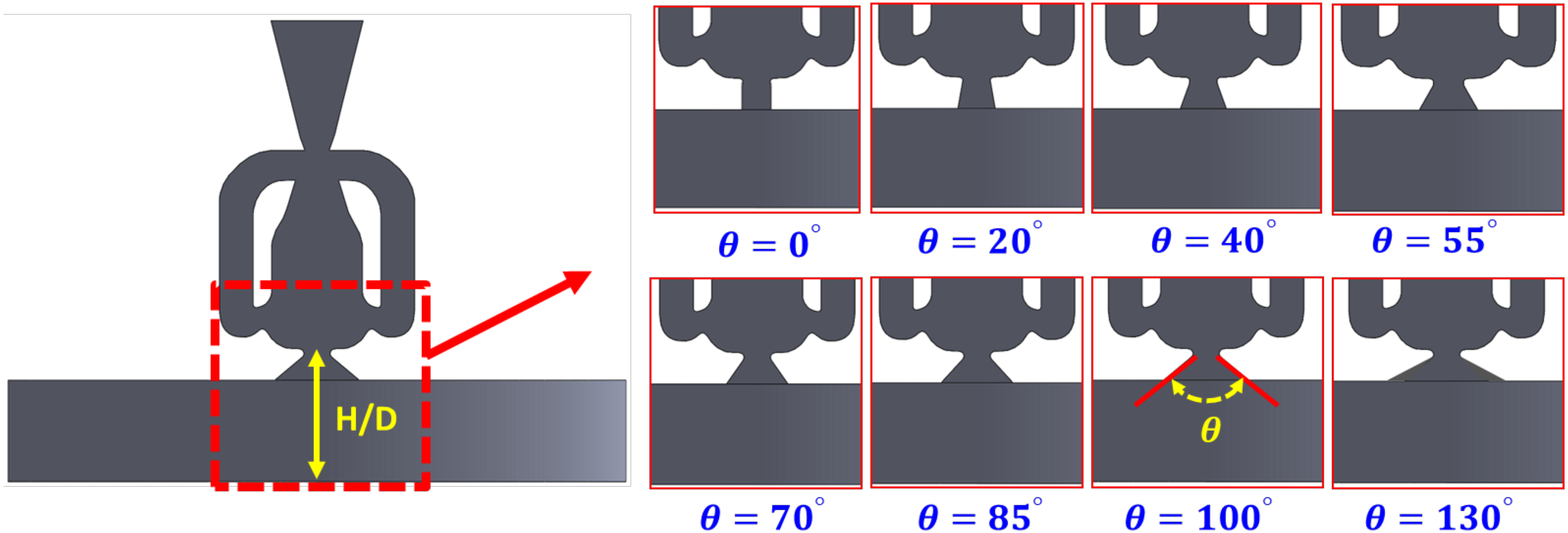

Effect of Exit Fan Angle (Time Averaged Nu)

- Data were averaged over 15 full oscillations for each case.
- The distribution of local *Nu* is very similar to a steady impinging jet at $\theta = 0^{\circ}$
- Two distinct peaks of local *Nu* can be seen at large exit fan angles ($40^{\circ} \leq \theta \leq 130^{\circ}$).
- The peak *Nu* location moves outward from the center (*x/D* = 0) as θ increases.

Time averaged Nu (H/D = 5, $\dot{m}_c$ = 100slpm)

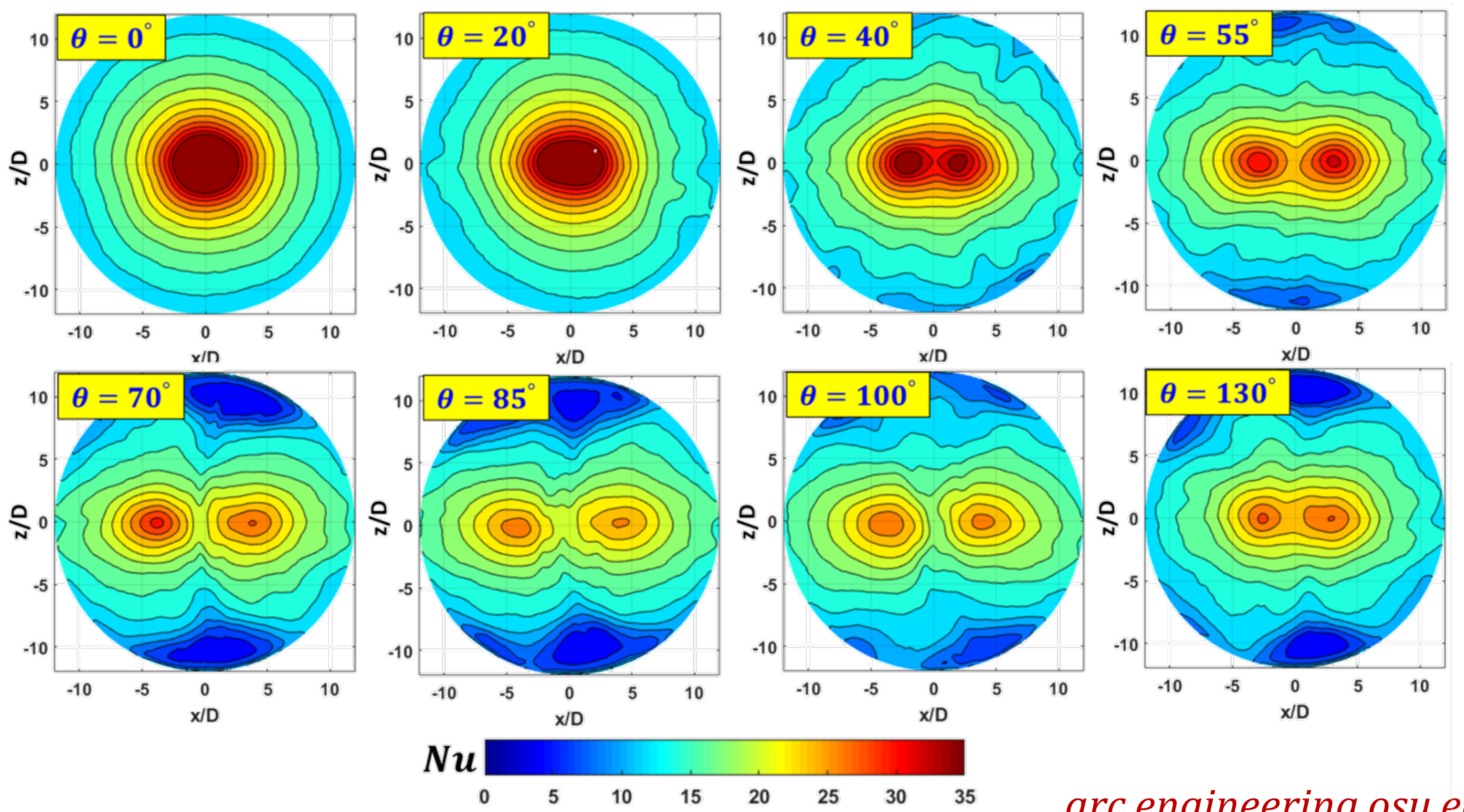

Effect of Exit Fan Angle (Time Averaged Nu)

- The geometric incidence can be estimated analytically by the jet-to-wall (H/D) distance and half angle ($\theta/2$) of the exit nozzle.
- A gray dashed line illustrates the ideal (1:1) relationship between geometric result and numerical prediction if the jet remains perfectly attached.
- The change in peak *Nu* location predicted by CFD is consistent with the geometric estimation for θ up to 70°

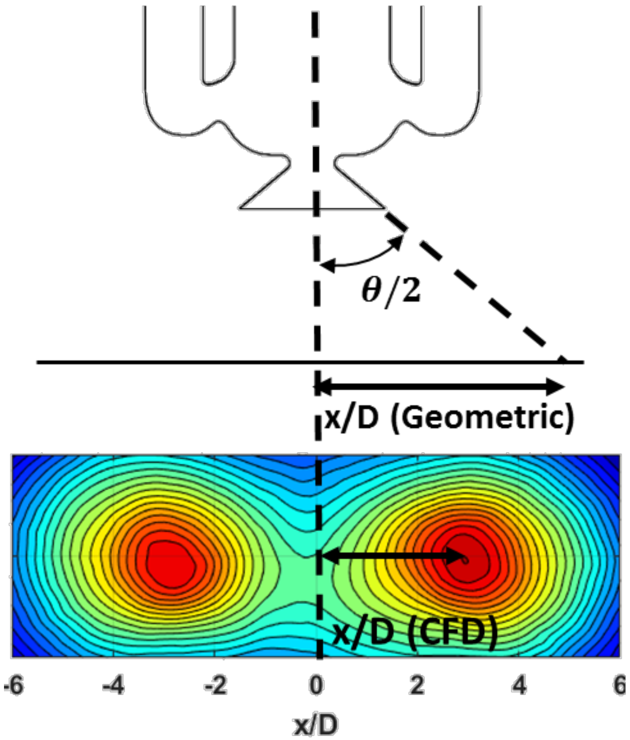

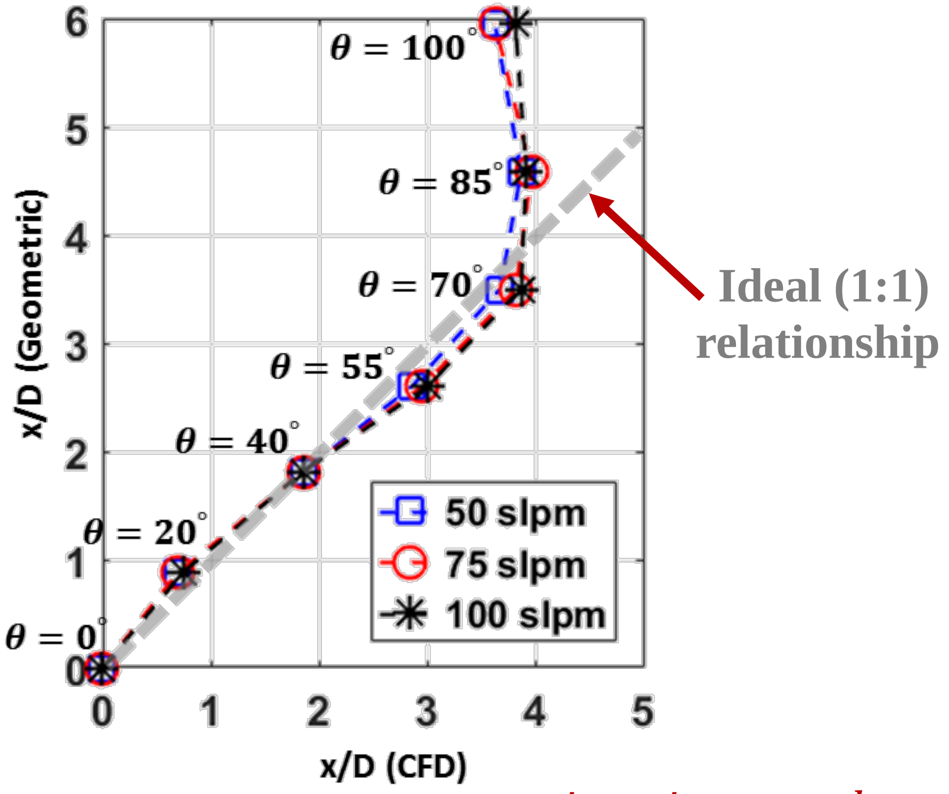

Effect of Exit Fan Angle (Time averaged flow field)

- Two separation bubbles start to appear at $\theta = 85^\circ$ and become much more pronounced at $\theta = 100^\circ$
- These separation bubbles are responsible for the local 'necking' that prevents the jet from spreading.

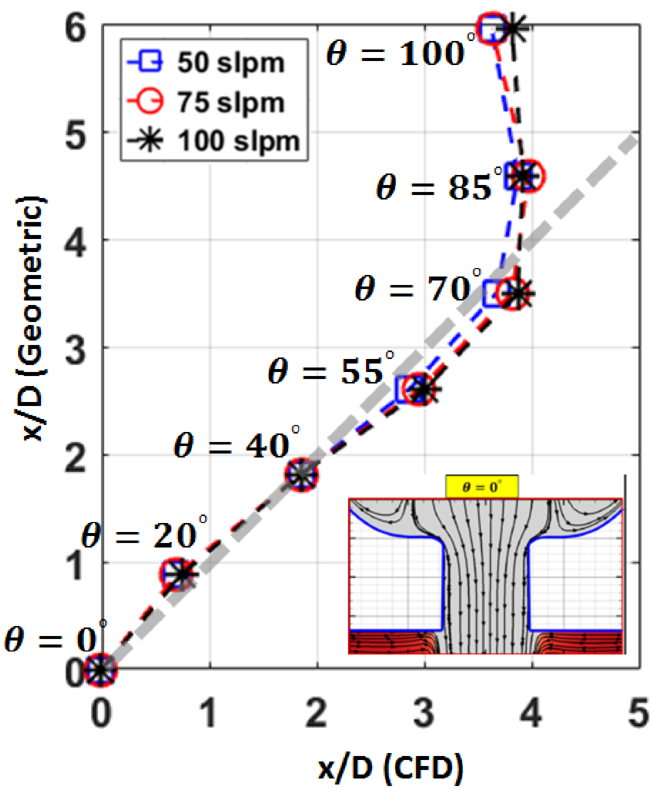

Time averaged velocity field and streamlines

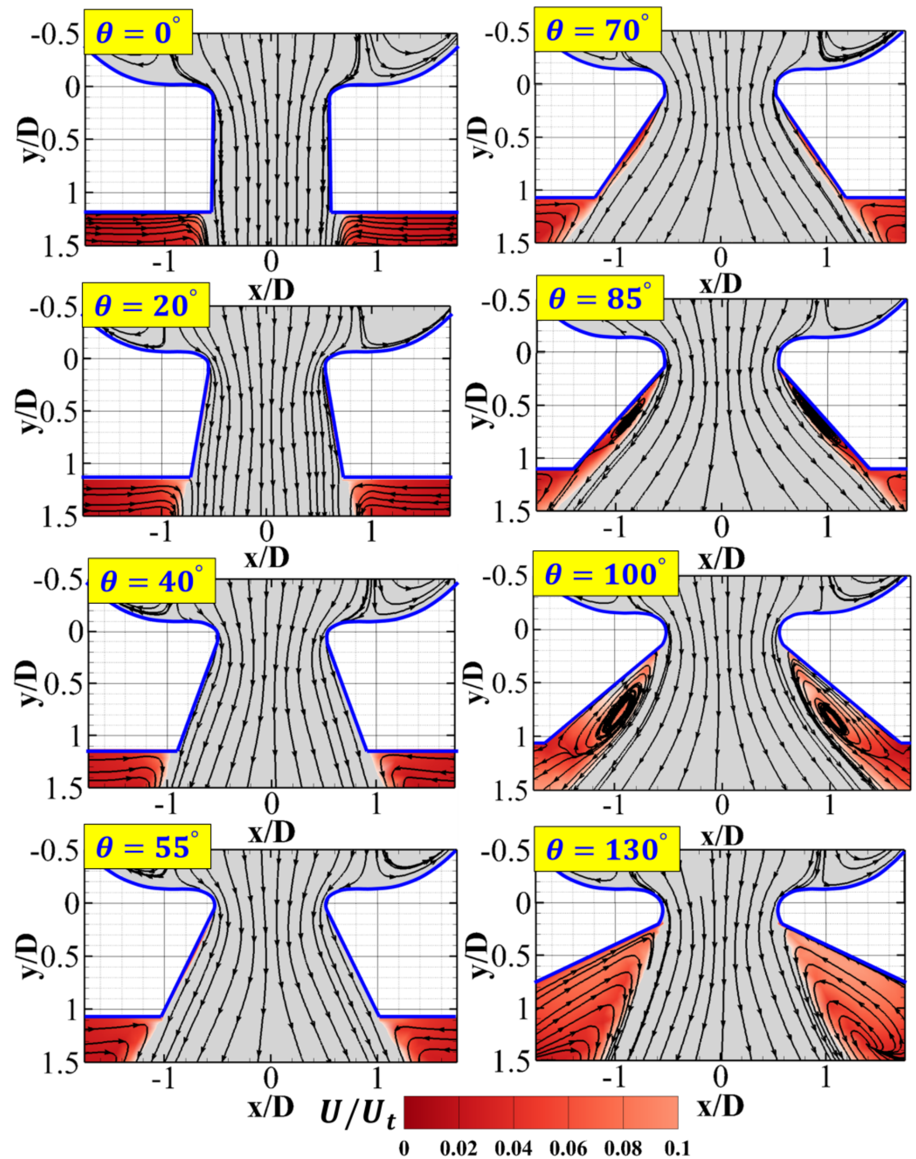

Effect of Exit Fan Angle (Averaged Nu and Cooling uniformity)

- The maximum area averaged ($\overline{Nu}$) was found at $\theta = 0^{\circ}$, and ($\overline{Nu}$) drops with the exit fan angles for all massflow rates.
- $\overline{Nu}$ reaches a minimum value at an exit angle somewhere around ($70^{\circ} < \theta < 100^{\circ}$).
- In order to show the actual benefit of the sweeping action, a new parameter was defined as '**Cooling Uniformity Index (λ)**'.
- $\boldsymbol{\lambda = 1}$ indicates a perfectly uniform surface temperature.

$$\lambda = 1 - \frac{\sum_{i=1}^{N} \sqrt{\left(Nu_i - Nu_{avg}\right)^2}\, A_i}{Nu_{avg}\, A}$$

- Cooling uniformity increases with massflow rate and exit fan angle (θ) at higher jet-to-wall spacing (H/D = 5 and 8).

Averaged Nu

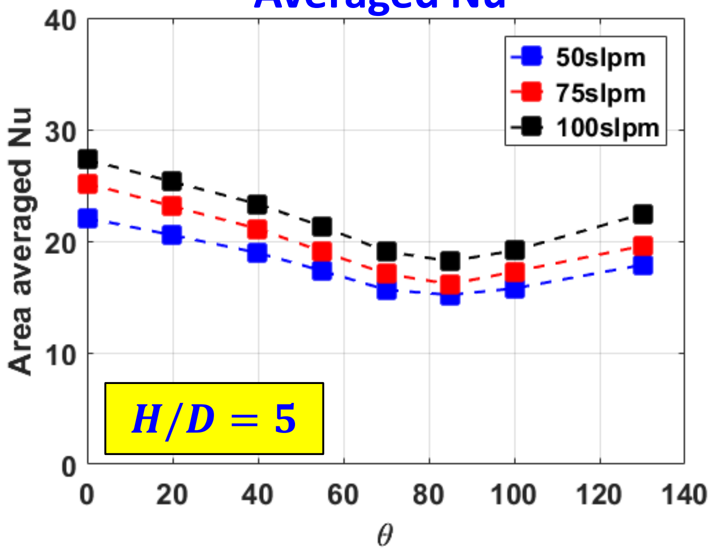

Cooling uniformity (λ)

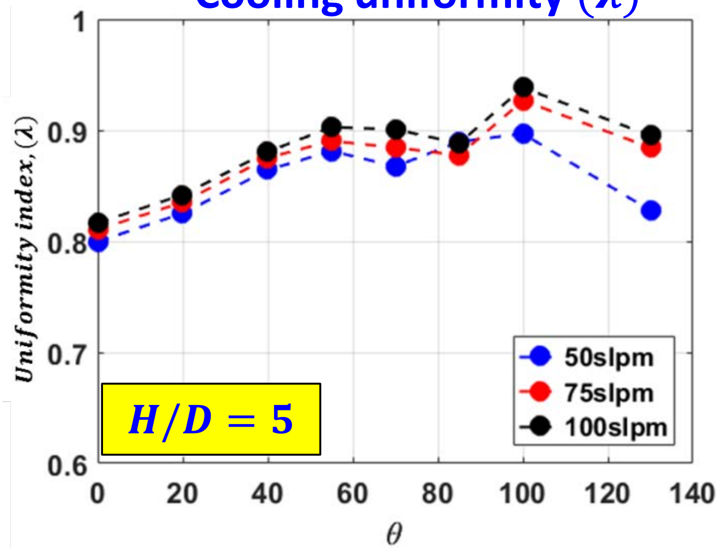

Vane Leading Edge Impingement (Vane geometry)

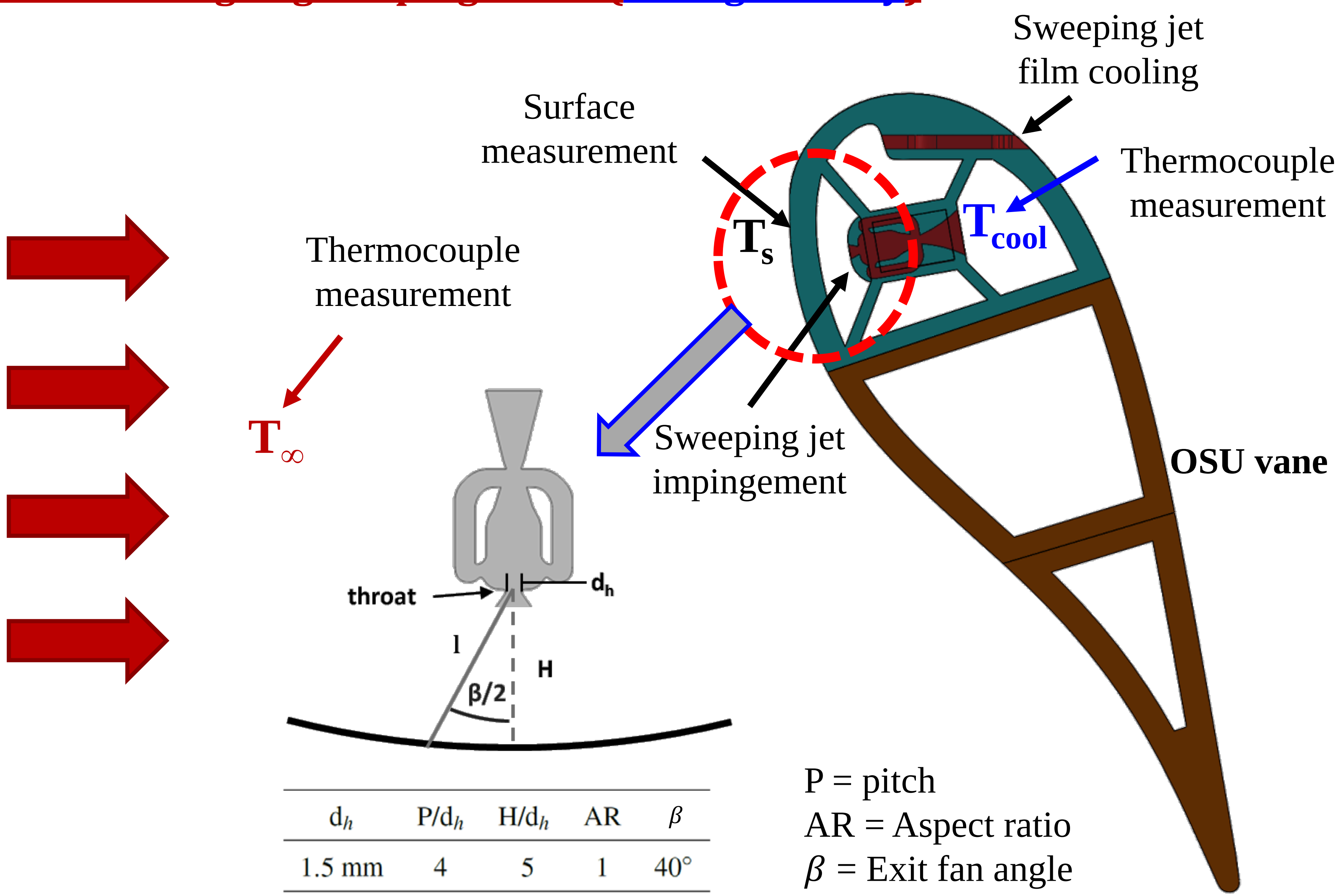

d_h	P/d_h	H/d_h	AR	β
1.5 mm	4	5	1	40°

P = pitch
AR = Aspect ratio
β = Exit fan angle

Vane Leading Edge Impingement (Internal Heat Transfer)

- Not enough information to solve for internal heat transfer coefficient directly.
- Computational **thermal inertia method** (Nirmalan et al. 2002)-
  1. Create solid model of leading edge.
  2. Apply known T_{∞} and T_{cool}.
  3. Apply assumed h_{ext}.
  4. Guess T_{int} to calculate h_{int}.
  5. Compare calculated $T_{s,ext}$ to measured $T_{s,ext}$.
  6. Update h_{int} based on the $T_{s,ext}$ discrepancy.
  7. Repeat 5,6 until convergence.

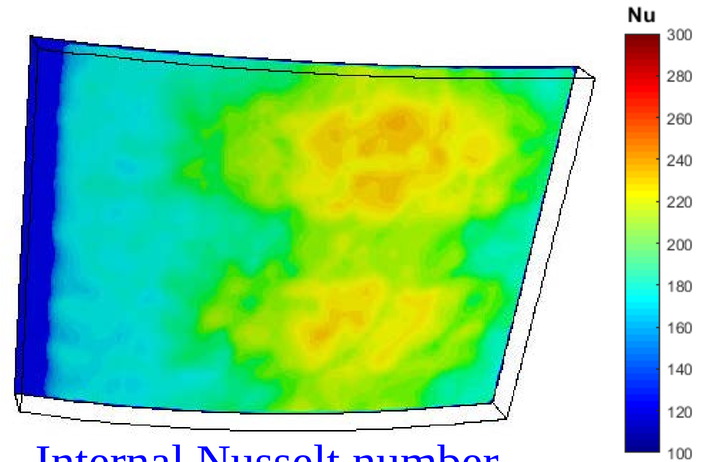

Internal Nusselt number (computed)

1 iteration

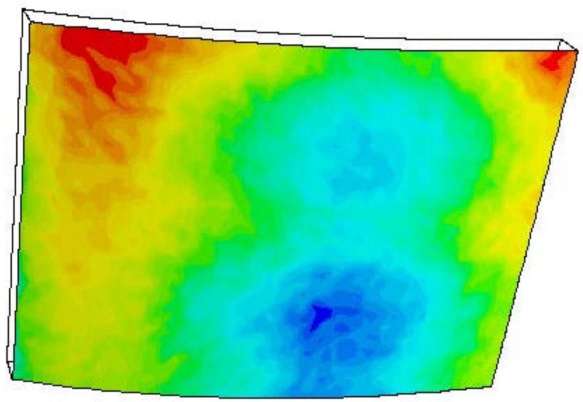

Surface Temperature (measured)

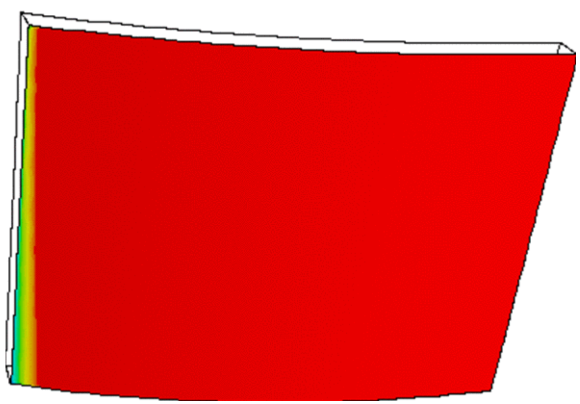

Surface Temperature (computed)

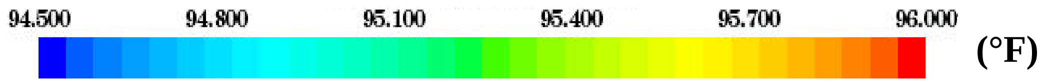

Vane Leading Edge Impingement (Preliminary results)

- Overall cooling effectiveness shows that sweeping jet underperformed compared to steady circular jet. However, sweeping jet shows uniform cooling.

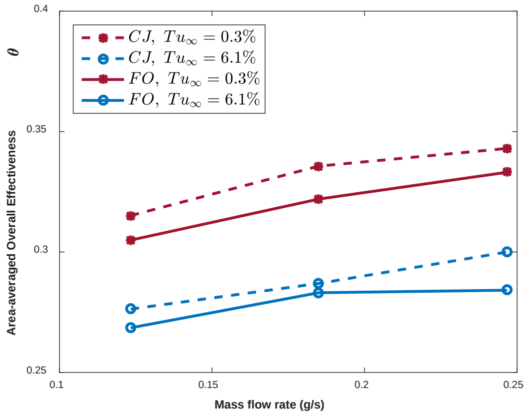

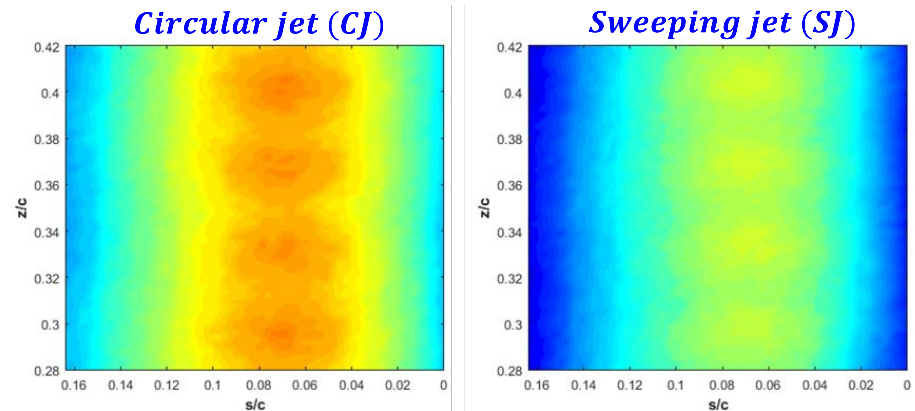

- Sweeping jet has higher pressure drop compared to steady jet.

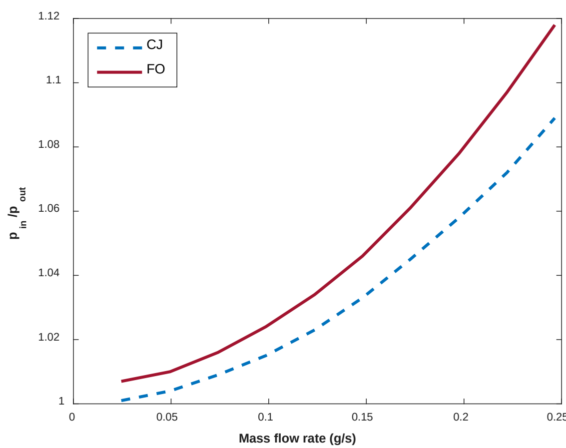

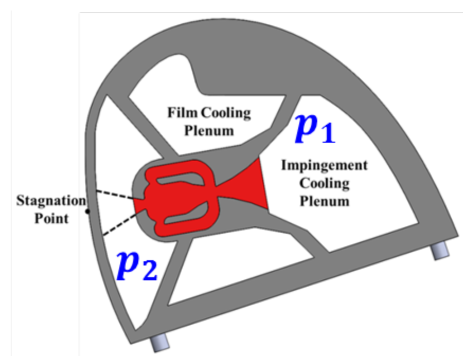

Sweeping jet (SJ)

82

Vane Leading Edge Impingement (Design iteration)

- Leading edge modules have identical:
  - Leading edge thickness (t)

- Modified leading edge modules have:
  - Film cooling hole exhaust schemes
  - Enlarged coolant supply plenum
  - Sharp edges are rounded

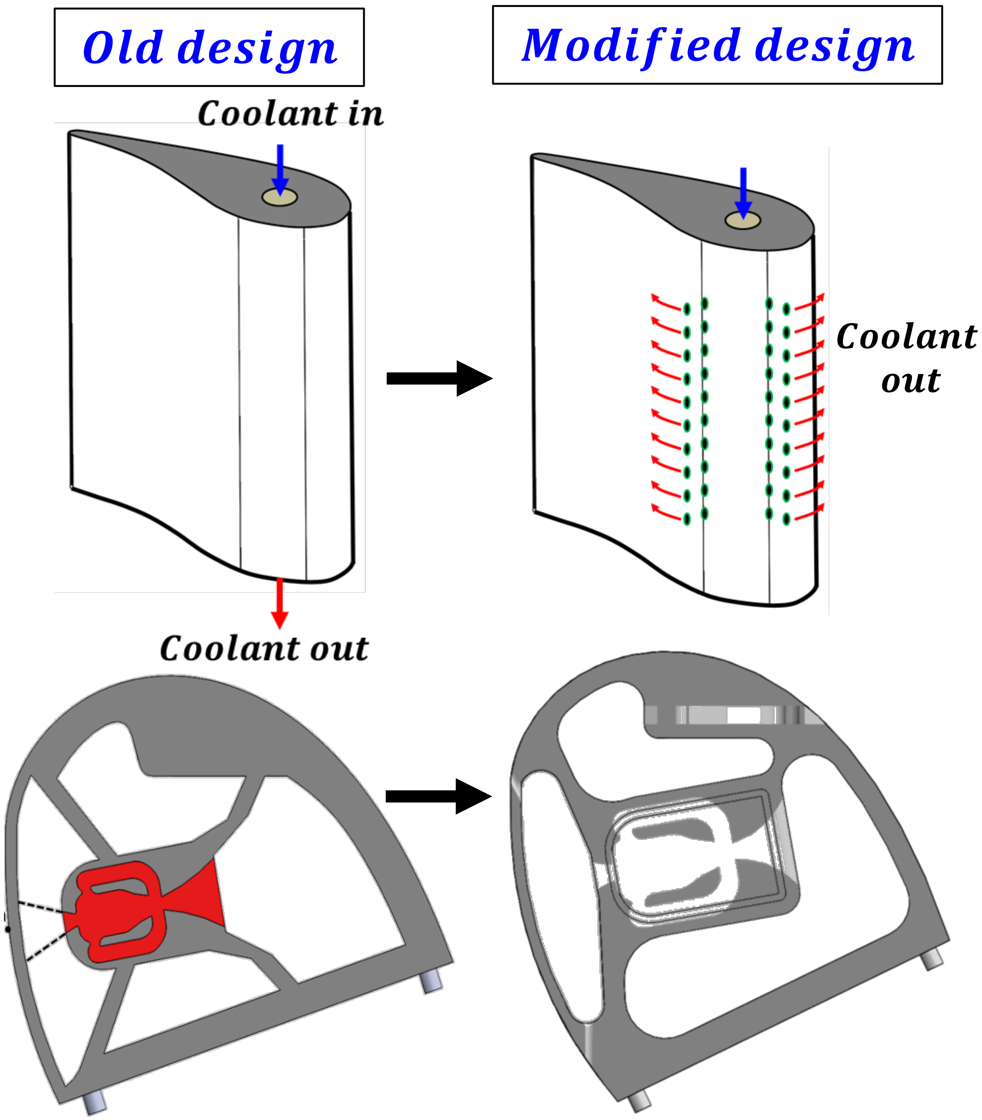

Geometry comparison

Parameter	*Old design*	*New design*
d_h	$1.55mm$	$2.37mm$
R/d_h	40.7	26.6
z/d_h	5	5
P/d_h	4	4
Number of jets	20	13

Vane Leading Edge Impingement (Overall Cooling Effectiveness)

- Overall effectiveness **averaged over central 10% of span.**
  - Expected trends with increasing coolant $\dot{m}$.
  - Sweeping jet provides less heat transfer.
  - Sweeping jet has a very uniform θ profile.

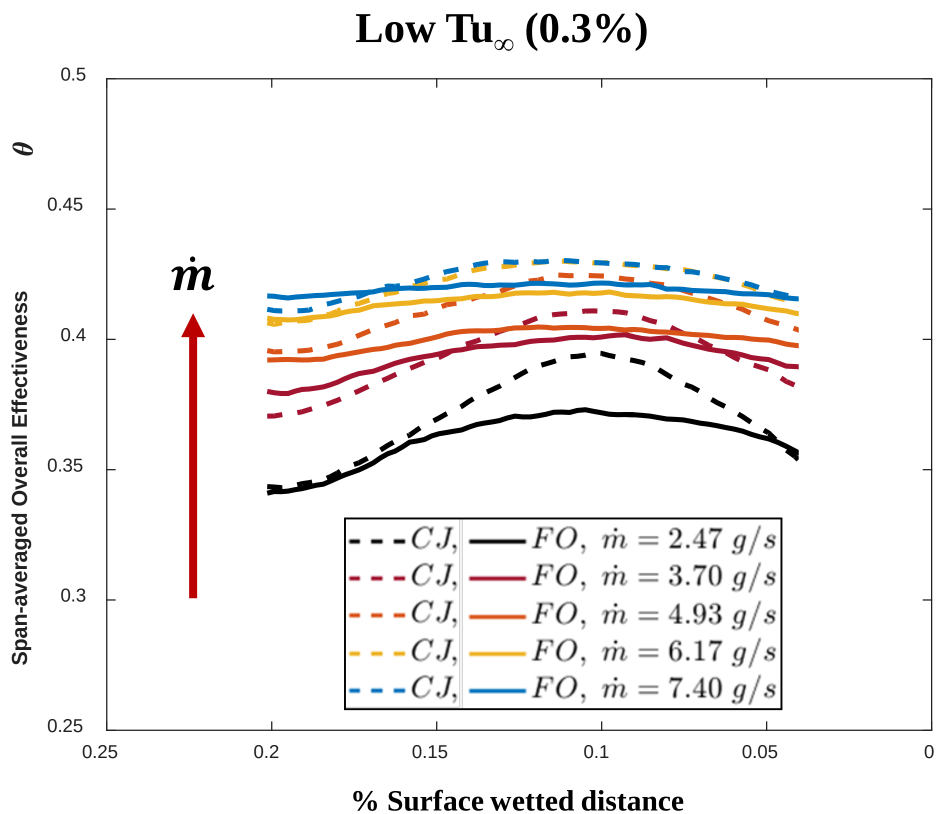

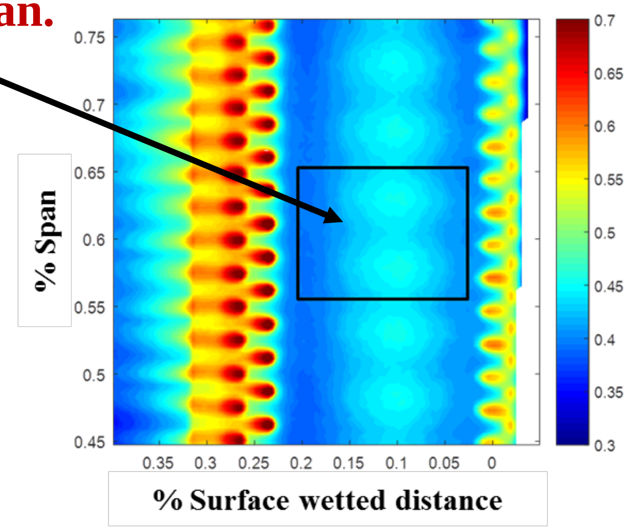

Vane Leading Edge Impingement (Cooling Uniformity)

- Heat transfer uniformity is quantified in terms of a new 'cooling uniformity index'
  - Uniformity index of 1 = constant heat transfer.
  - Sweeping jet heat transfer is **more uniform**.

$$\textbf{Uniformity Index} = 1 - \frac{\sum_{i=1}^{n}\sqrt{(\theta_i-\bar{\theta})^2}A_i}{\bar{\theta}A}$$

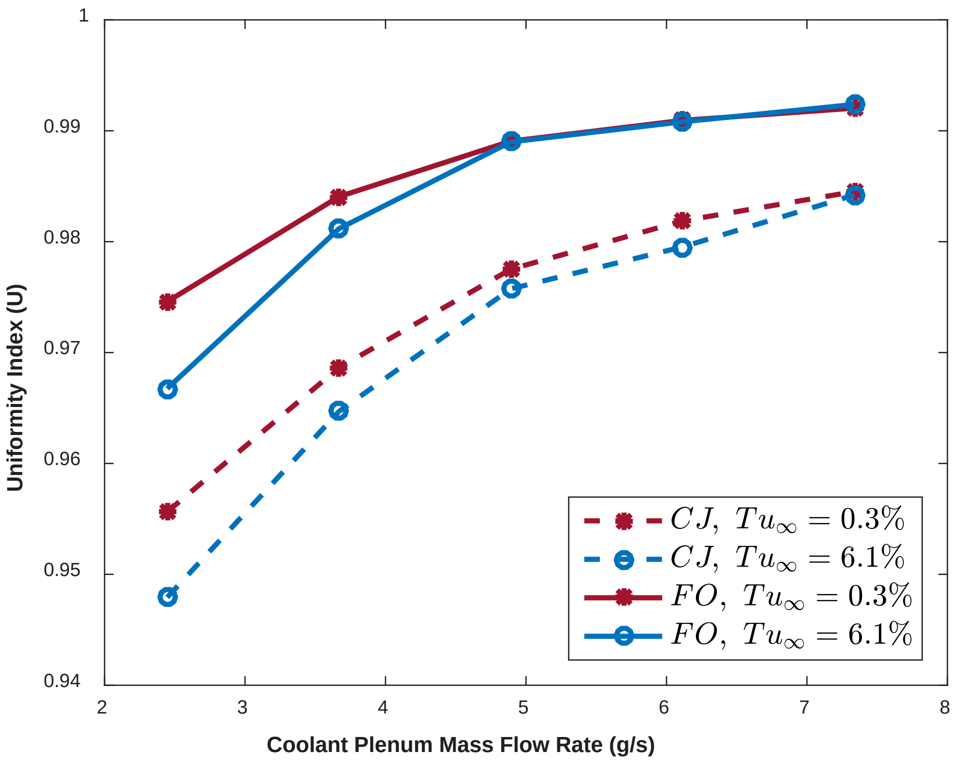

Vane Leading Edge Impingement (Pressure drop)

- **Sweeping jets drop no additional pressure.**
  - Additive manufacturing allows for smoothed internal features.
  - Unsteady jet plenumization has no effect on film cooling hole pressure drop.

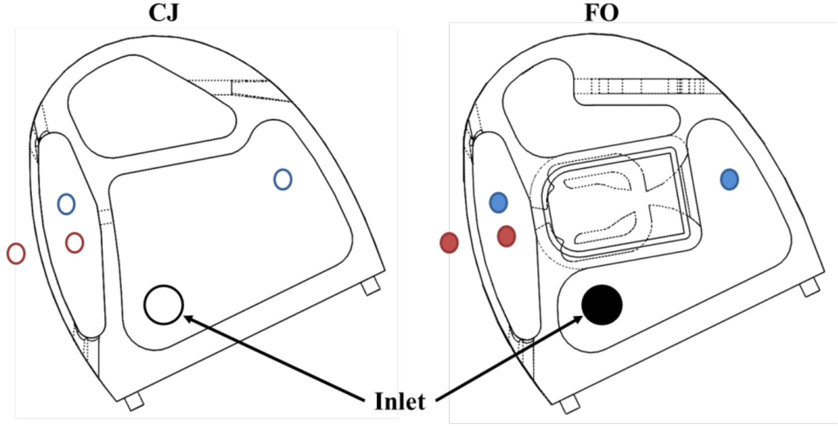

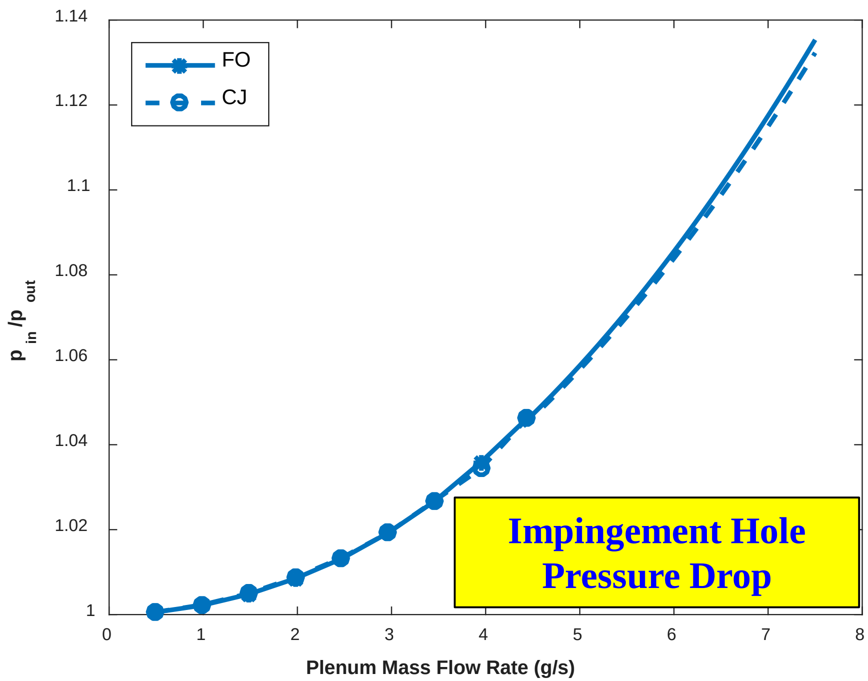

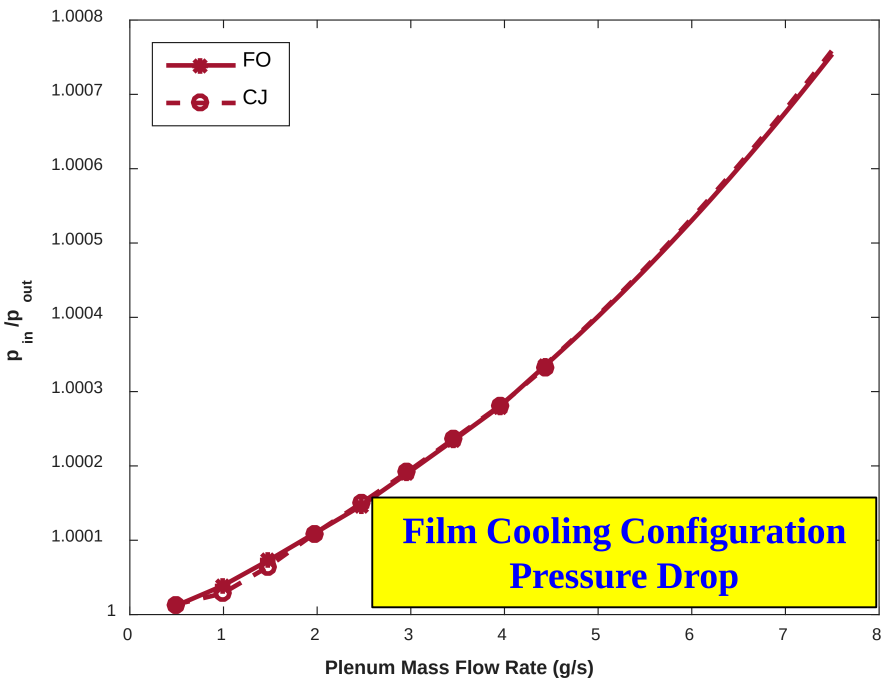

What's Next?

- Complete transonic cascade testing
  - LE impingement cooling
  - Triangular pins in TE cooling
  - Explore effect of high turbulence

- Design, fabricate and test DMLS parts for High Temperature Cascade testing

Publications

1. 2 more papers submitted for IGTI 2019
2. Asar, M.E., Agricola, L.M., Hossain, M.A., and Bons, J.P., 2018, “An Innovative Pin Fin Design for Turbine Trailing Edge Cooling”, presented at the July 2018 AIAA Propulsion and Energy Forum, Cincinnati, OH. Paper #: AIAA-2018-XXXX.
3. Hossain, M.A., Agricola, L.M., Ameri, A., Gregory, J.W., and Bons, J.P., 2018, “Effects of Exit Fan Angle on the Heat Transfer Performance of Sweeping Jet Impingement”, presented at the July 2018 AIAA Propulsion and Energy Forum, Cincinnati, OH. Paper #: AIAA-2018-XXXX.
4. Hossain, M.A., Agricola, L., Ameri, A., Gregory, J.W., Bons, J.P., 2018, “SWEEPING JET IMPINGEMENT HEAT TRANSFER ON A SIMULATED TURBINE VANE LEADING EDGE”, Journal of Global Power and Propulsion Society (GPPS), 2018, 2:402-414.
5. Hossain, M.A., Prenter, R., Lundgreen, R., Ameri, A., Gregory, J.W., Bons, J.P., 2017, "Experimental and numerical investigation of sweeping jet film cooling," ASME Journal of Turbomachinery, 140(3), p. 031009
6. Agricola, L., Hossain, M.A., Ameri, A., Gregory, J.W., and Bons, J.P., 2018, “Turbine Vane Leading Edge Impingement Cooling with a Sweeping Jet,” presented at the IGTI 2018 conference in Oslo, Norway. (GT2018-77073)
7. Hossain, M.A., Agricola, L., Ameri, A., Gregory, J.W., and Bons, J.P., 2018, “Sweeping Jet Film Cooling on a Turbine Vane,” presented at the IGTI 2018 conference in Oslo, Norway. (GT2018-77099)
8. Hossain, M.A., Agricola, L., Ameri, A., Gregory, J.W., Bons, J.P., 2018, “SWEEPING JET IMPINGEMENT HEAT TRANSFER ON A SIMULATED TURBINE VANE LEADING EDGE”, presented at Global Power and Propulsion Society (GPPS) Forum 18, in Montreal, Quebec, Canada, 7-9 May 2018. (GPPS-2018-0148)
9. Hossain, M.A., Prenter, R., Lundgreen, R.K., Ameri, A., Gregory, J.W., and Bons, J.P., 2017, “Experimental and Numerical Investigation of Sweeping Jet Film Cooling,” presented at the ASME Turbo Expo 2017 in Charlotte, SC, June 26-30, 2017, (GT2017-64479).
10. Prenter, R., Hossain, M.A., Agricola, L., Ameri, A., and Bons, J.P., 2017, “Experimental and Numerical Characterization of Reverse-Oriented Film Cooling,” presented at the ASME Turbo Expo 2017 in Charlotte, SC, June 26-30, 2017, (GT2017-64731).
11. Hossain, M.A., Agricola, L., Ameri, A., Gregory, J.W., and Bons, J.P., 2018, “Effects of Curvature on the Performance of Sweeping Jet Impingement Heat Transfer,” presented at AIAA SciTech 2018 in Kissimmee, FL, Jan 8-12, 2018. Paper #: AIAA-2018-0243.
12. Agricola, L., Hossain, M.A., Prenter, R., Lundgreen, R.K., Ameri, A., Gregory, J.W., and Bons, J.P., 2017, “Impinging Sweeping Jet Heat Transfer,” presented at the 2017 AIAA Joint Propulsion Conference, July 10-12, 2017 in Atlanta, GA. Paper #2017-4974.
13. Hossain, M.A., Prenter, R., Lundgreen, R., Agricola, L., Ameri, A., Gregory, J.W., and Bons, J.P., 2017, “Investigation of Crossflow Interaction of an Oscillating Jet,” presented at AIAA SciTech Conference, Jan 9-13, 2017, Grapevine, TX, paper #AIAA-2017-1690.
14. Hossain, M.A., Prenter, R., Agricola, L., Lundgreen, R., Ameri, A., Gregory, J.W., and Bons, J.P., 2017, “Effects of Roughness on Performance of Fluidic Oscillators,” presented at AIAA SciTech Conference, Jan 9-13, 2017, Grapevine, TX, paper #AIAA-2017-0770.

Questions?